J. Fluid Mech. (1988), *vol.* 193, *pp.* 303–345
Printed in Great Britain

The bursting sequence in the turbulent boundary layer over progressive, mechanically generated water waves

By YIANNIS ALEX PAPADIMITRAKIS†, ROBERT L. STREET‡ AND EN YUN HSU‡

† Goddard Space Flight Center, Code 671, Greenbelt, MD 20771, USA

‡ Environmental Fluid Mechanics Laboratory, Department of Civil Engineering, Stanford University, Stanford, CA 94305, USA

(Received 1 June 1983 and in revised form 31 December 1987)

The structure of the pressure and velocity field in the air above progressive, mechanically generated water waves was investigated in order to evaluate the influence of a mobile and deformable boundary on turbulence production and the related bursting phenomena. The Reynolds stress fluctuations were measured in a transformed Eulerian wave-following frame of reference, in a wind-wave research facility at Stanford University.

The structure of the wave-coherent velocity field was found to be very sensitive to the height of the critical layer below which the waves travel faster than the wind. Because the critical-layer height changes rapidly with the ratio (c/u_*) of the wave speed to the wind friction velocity, the structure of the wave-coherent velocities depends strongly on the parameter c/U_{δ_0}, where U_{δ_0} is the mean free-stream wind velocity. When the critical height is large enough that most of the flow in the turbulent boundary layer is below the critical height, the structure of the wave-coherent velocities is strongly affected by the Stokes layer (in the air), which under the influence of turbulence can have thickness comparable with the wave amplitude. In contrast, when the critical height is small enough that most of the flow in the boundary layer is above the critical height, the structure of the wave-coherent velocities is strongly affected by the critical layer. The latter was found to be nonlinear and turbulently diffusive.

The dependence of the structural behaviour of the wave-coherent velocity field upon the critical and Stokes layers results in considerable modifications of the turbulence-generating mechanism during the bursting-cycle, as the dimensionless wave speed c/U_{δ_0} changes. Such modifications are manifested by an enhancement of the contributions to the mean Reynolds stress of the bursting events (relative to their solid-wall counterparts), and their dependence on the dimensionless wave speed. For $c/U_{\delta_0} \geqslant 0.68$ (or $c/u_* > 20$), the nonlinear critical-layer thickness is large compared to the wave amplitude (except when $c/U_{\delta_0} = 0.68$), and the diffused Stokes layer stimulates the wave-associated stress production. In the water proximity, the bursting contributions remain nearly constant with dimensionless wave speed; ejections account for 90% of the mean Reynolds stress, whereas sweeps provide 77%, the excess over 100% being balanced by the outward and inward interactions. For $c/U_{\delta_0} < 0.68$, the critical-layer thickness is smaller than the wave amplitude and all contributions increase gradually with c/U_{δ_0}. However, the ratio of ejection to sweep contributions remains unaltered and ≈ 1.15, indicating that sweeps are nearly as energetic as ejections at all dimensionless wave speeds. The value of $c/U_{\delta_0} \approx 0.68$

appears to separate the flow regimes of high and low critical level, respectively, where significant and weak production of the wave-associated stresses have been found. Near the water surface the height distribution of the fractional contributions of the bursting events is also sensitive to the ratio c/U_{δ_0}. In the equilibrium region of the boundary layer it remains uniform and in the free stream rises sharply, independent of dimensionless wave speed.

The mean time period between ejections or sweeps depends on both the wave and wind field characteristics and does not scale with either the inner or the outer flow variables. The former can be determined from the time between the first two largest consecutive peaks of the phase-averaged Reynolds stress distribution.

In the water proximity, the height distribution of the normalized energy production is sensitive to c/U_{δ_0}; only when $c/U_{\delta_0} \geqslant 0.68$ does it show a peak of increasing magnitude with increasing dimensionless wave speed.

1. Introduction

1.1. *Bursting and Reynolds stress production over solid boundaries*

In a turbulent boundary layer, turbulence generation plays a primary role in determining the local balance of production, transport and dissipation of turbulent kinetic energy and, hence, it is important that the mechanism(s) of Reynolds stress generation be well understood. Considerable theoretical and experimental work, using flow visualization and either velocity or pressure sensors, has been done for wall flows (Kline *et al.* 1967; Corino & Brodkey 1969; Kim, Kline & Reynolds 1971; Grass 1971; Wallace, Eckelmann & Brodkey 1972; Offen & Kline 1975). Hinze (1975), Laufer (1975) and Willmarth (1975) have written reviews describing the status of research on solid-wall turbulence, especially on the bursting phenomena of turbulent boundary layers. Experimental investigations of these phenomena have disclosed a complex quasi-ordered flow structure which consists of a deterministic sequence of fluid motions occurring randomly in space and time. These studies generally concentrate on determining the average spatial and temporal scales of ejection and sweep events, the two most distinct features of the quasi-ordered structures. Although the spatial configuration and scales of the wall structure are generally agreed upon by the different investigators, there is considerable disagreement concerning the frequency of occurrence and the scaling of the bursting events in bounded shear flows. Bogard & Tiederman (1983) presented results for the non-dimensional mean bursting period (normalized with the inner and/or outer flow variables) as a function of Reynolds number, obtained by different investigators and corresponding to various flows, including flow visualization and probe data. These non-dimensional bursting periods show large scatter. For the probe data, the scatter extends over a Reynolds-number range greater than an order of magnitude. Perhaps of greater significance are the different trends found in these results. The average bursting period of the probe data shows an effective increase with increasing Reynolds number, whereas for the flow visualization results this period decreases or at least remains unchanged with increasing Reynolds number. These differences have been attributed to the different detection schemes used, but Bogard & Tiederman (1983) suggested that probe measurements probably detect something different from the bursts identified using flow visualization techniques. Blackwelder & Haritonidis (1983) concluded that the discrepancies among the probe data can be attributed to the sensor size and proposed a correction scheme for the measured non-dimensional mean bursting frequency, scaled with the inner variables, applicable wherever the

viscous length† of the detecting probe is greater than 20. Alfredsson & Johansson (1983), however, pointed out that the correction scheme of Blackwelder & Haritonidis (1983) contains no dependence on the averaging time used by the variable-interval time-averaging (VITA) method (Blackwelder & Kaplan 1972) to detect bursting. Therefore, it cannot explain the trend seen in their data, which display the frequency of occurrence of VITA (bursting) events as a function of the integration time, obtained from two probes with viscous lengths of 13 and 32, respectively.

In previous investigations (Offen & Kline 1975; Tiederman, Smith & Oldaker 1977) a distinction was made between ejections and the overall process of a streak breakup, which was called a burst. Recent experimental evidence (Bogard & Tiederman 1986) further supports the idea that groups of ejections are related to the breakup of a single streak. As a result, in the recent literature the term 'bursting period' has been replaced by the term 'ejection period', indicating that a single burst may contain more than one ejection grouped closely together. The interested reader should peruse Offen & Kline (1975) and Hinze (1975, pp. 660 ff.) for a physical description of streaks. Briefly, the 'wall streak' is a basic flow module that can be viewed as a sub-boundary layer, within the conventionally defined boundary layer, consisting of many streaklines. The lift-up stage of bursting can, in turn, be viewed either as an upwelling motion of this sub-boundary layer (a process similar to a local, convected separation) or, equivalently, as a consequence of vortex roll-up. Sweeps are thought to represent the passage of a previous burst from further upstream. According to Schraub *et al.* (1965), a streakline is defined as the locus of points connecting all particles that have passed through a given fixed point in space. Only in steady flows do streaklines coincide with streamlines. In flows over solid boundaries streaks have a wavy shape, although sometimes one can also observe a local spiral motion in the streamwise direction (see also §3.2.2). The wave motion is more distinct in the vertical plane close to the wall, whereas the spiral motion is more distinct at greater distances from the wall.

1.2. *Bursting and Reynolds stress production above an air–water interface*

Past field and laboratory measurements of the velocity and pressure fields over water waves, conducted by Elliott (1972), Shemdin & Lai (1973), Snyder *et al.* (1981); Hsu, Hsu & Street (1981); Kawamura *et al.* (1981); Kawai (1981, 1982); Hsu & Hsu (1983); Papadimitrakis, Hsu & Street (1984); Papadimitrakis, Hsu & Wu (1987) and others, have shown considerable alteration of the wind turbulence owing to the presence of waves. Most of the observational evidence of these changes has been in the form of spectra of velocity, pressure and, in a few cases, temperature and humidity fluctuations (see, for example, Antonia & Chambers 1980; Papadimitrakis, Hsu & Wu 1986). Distinct peaks, for example, have been found in the power spectral densities of pressure and vertical as well as horizontal velocities, near the frequency at which the spectral density of the surface-wave displacement is maximum. Wave-coherent contributions to the mean Reynolds stress (abbreviated hereinafter as w.c., see §2 for pertinent definitions) have also been found to cause reduction of the latter by as much as 25% at large ratios of c/U_{δ_0} (i.e. $\geqslant 1$), a condition common for the dominant waves in the open ocean (Chambers & Antonia 1981). Moreover, Kitaigorodskii & Donelan (1984) have argued that the turbulence structure of the air in the water proximity is affected by the surface roughness condition, particularly at low values of c/U_{δ_0}, as flow separation from steep (generally small) roughness

† Defined as $l^+ = lu_*/\nu$, where l, u_* and ν are probe length, friction velocity, and kinematic viscosity of the air, respectively.

elements enhances the surface turbulence. Therefore, it will be of great importance to know the characteristics of the bursting cycle in the presence of a mobile and deformable boundary.

Among these and other investigations on the structure of turbulent air flows above water waves, only a few have explored the Reynolds stress production mechanism in the water proximity (Mollo-Christensen 1973; Takeuchi, Leavitt & Chao 1977; Chambers & Antonia 1981; Kawamura *et al.* 1981; Toba, Kawamura & Okuda 1984; Warhaft & Bolgiano 1984; and Kawamura & Toba 1985). These studies give direct evidence for intermittent momentum and heat exchange in the lower and inner part of either the atmospheric or a laboratory boundary layer above water waves, and show that the near-surface stress is mainly supported by intermittent bursts. Dorman & Mollo-Christensen (1973) associated the bursts of surface stress with the generation of capillary waves observed near the crest of the dominant waves. They further suggested that these bursts occur preferentially at some phases of the large-scale wave field and play an important role in the generation processes of large sea surface waves. The existence of bursting phenomena over wind waves, characterized by the intermittent outflow and inflow of low- and high-speed air parcels has been reported by Kawai (1981, 1982) and Kawamura *et al.* (1981). Their visual observations revealed ordered structures in the air with a horizontal lengthscale comparable with the dominant wavelength. They also showed that these ascending and descending motions, associated with large negative spikes in the time series of instantaneous Reynolds stress, occur at relatively fixed positions on the windward and leeward side of the dominant wave crests. This abrupt Reynolds stress generation by the coupling of horizontal and vertical velocity fluctuations is, certainly, similar to the ejection and sweep stages of the bursting phenomena found in flows over solid walls. According to Csanady (1985), these shear stress spikes over wave crests act as the principal instrument of air–sea momentum transfer.

This paper describes the influence of nearly sinusoidal, mechanically generated water waves on the turbulent Reynolds stress production mechanism and on the bursting-related phenomena in the air flow above them. Comparison is made with the results of Lu & Willmarth (1973) for flows over smooth flat walls, Nakagawa & Nesu (1977, 1981) for open-channel flows over smooth and rough beds, and Takeuchi *et al.* (1977); Kawamura *et al.* (1981) and Kawamura & Toba (1985) for flows with mechanically and/or wind-generated waves. Additional information regarding the mean periods and scales of ejections and sweeps, as well as the wave-associated (abbreviated hereinafter as w.a.) and small-scale turbulent energy production, is also presented. The role of w.c. pressure fluctuations in the bursting sequence under the present conditions is examined in a separate paper.

2. Experimental apparatus and data analysis

The experiments were conducted in the Stanford Wind-Wave Research Facility (see Papadimitrakis *et al.* 1985). The data acquisition station was located 13 m from the air inlet. The depth of the air flow $H(= 2\delta_0)$, measured from the mean water level to the channel roof, was 1.07 m. The water depth d was 0.83 m. The 1 Hz, mechanically generated wave was in deep water with a nominal amplitude $a = 2.54$ cm, a wavelength $L = 1.56$ m, and a wavenumber $k = 4.03$ m^{-1}.

The air flow above the progressive, small-amplitude (wave slope ≈ 0.1), sinusoidal water wave is considered to be two-dimensional (see Papadimitrakis *et al.* 1986). In the Cartesian coordinate system used here, x is taken in the wave propagation or

mean air flow direction and y is the vertical coordinate measured upward from the mean water level. The coordinate transformation used contains only vertical translation, namely

$$t = t^*; \quad x = x^*; \quad y = y^* + f(y^*)\,\tilde{\eta}, \tag{2.1a, b, c}$$

$$f(y^*) = \sinh(kH - ky^*)/\sinh(kH), \tag{2.2}$$

and has been described by Hsu *et al.* (1981); $\tilde{\eta}$ represents the sinusoidal water surface displacement from the mean water level. To measure the flow quantities in the transformed wave-following frame, the wave-follower system described in Papadimitrakis *et al.* (1984) (referred to, hereinafter as I) was used as the primary instrument. The X hot film and wave-height gauge characteristics, their calibrations and accuracies are also discussed there.

The air and water flows were permitted to settle into statistical equilibrium over a half-hour period prior to data acquisition. The data taken correspond to seven mean free-stream wind velocities in the range 140–400 cm/s. They were collected at 20 or 21 elevations, 0.75–53.3 cm (± 0.25 mm) above the instantaneous water surface.

Since the instantaneous velocity field above the waves consists of a mean, a w.c. perturbation, and a turbulent component, namely

$$u_i = U_i + \tilde{u}_i + u_i'; \quad i = 1, 2, \tag{2.3}$$

familiar time and phase averages were used to extract the w.c. fluctuations from the total signals. The phase average contains only the mean and w.c. parts; therefore

$$\tilde{u}_i = \langle u_i \rangle - U_i, \tag{2.4}$$

where $U_i(U, 0)$ is the time-averaged mean velocity, $\tilde{u}_i(\tilde{u}, \tilde{v})$ is the w.c. perturbation, $u_i'(u', v')$ is the turbulence fluctuation, and $\langle\ \rangle$ denotes phase averaging. The vertical w.c. velocity was corrected to account for the spurious component introduced by the wave-follower motion (see Hsu *et al.* 1981).

The bursting events were identified by classification of the measured Reynolds stress uv according to the Quadrant technique, that is, according to the signs of $u\,(= \tilde{u} + u')$ and $v\,(= \tilde{v} + v')$ signals. Brodkey, Wallace & Eckelmann (1974) termed $u < 0, v > 0$ an ejection; $u > 0, v < 0$ a sweep; $u < 0, v < 0$ a wallward interaction; and $u > 0, v > 0$ an outward interaction. This terminology is also used here. Therefore, ejections and sweeps are always associated with the second and fourth quadrants of the (u, v)-plane, respectively. Contributions to the mean Reynolds stress $\overline{uv}$ from the four quadrants of the (u, v)-plane were computed as outlined by Lu & Willmarth (1973); here the overbar indicates time averaging. The contribution to $\overline{uv}$ from the region of the ith quadrant, denoted by $\overline{uv}_i$, is such that

$$\frac{\overline{uv}_i}{\overline{uv}} = \frac{1}{\overline{uv}} \frac{1}{T} \int_0^T uv(t)\, S_i(t)\, \mathrm{d}t, \tag{2.5}$$

where T is the record length, and $S_i(t)$ is an on–off function defined as,

$$S_i(t) = \begin{cases} 1, & \text{when the point } u, v \text{ is in the } i\text{th quadrant,} \quad (2.6a) \\ 0, & \text{otherwise,} \quad (2.6b) \end{cases}$$

$\overline{uv}_2$ and $\overline{uv}_4$ correspond to the ejection and sweep quadrants, whereas $\overline{uv}_1$ and $\overline{uv}_3$ correspond to the interaction quadrants.

The phase-averaged Reynolds stress is approximately equal to the sum of phase-averaged w.a., $\langle \tilde{u}\tilde{v} \rangle$, and turbulent, $\langle u'v' \rangle$, stresses, namely

$$\langle uv \rangle \approx \langle \tilde{u}\tilde{v} \rangle + \langle u'v' \rangle \tag{2.7}$$

provided that $\tilde{u}, \tilde{v}$ are uncorrelated with u', v' and $\langle \tilde{u}v' \rangle, \langle \tilde{v}u' \rangle$ are small. Therefore, in flows above water waves it is important to study the behaviour of the total phase-averaged stress $\langle uv \rangle$ as well as that of either $\langle \tilde{u}\tilde{v} \rangle$ or $\langle u'v' \rangle$. Classification of these stresses may provide insight into the effect of a mobile and deformable boundary on the mechanism of turbulent energy production and its partition among the various fields. Contributions to the mean w.a. stress $\overline{\tilde{u}\tilde{v}}$ from the four quadrants of the $\langle \tilde{u} \rangle, \langle \tilde{v} \rangle$- (or $(\langle u \rangle, \langle v \rangle)$)-plane were computed in a similar fashion. The contribution to this stress from the region of the ith quadrant, denoted by $\overline{\tilde{u}\tilde{v}}_i$, is such that

$$\frac{\overline{\tilde{u}\tilde{v}}_i}{\overline{\tilde{u}\tilde{v}}} = \frac{1}{\overline{\tilde{u}\tilde{v}}} \frac{1}{T_w} \int_0^{T_w} \langle \tilde{u} \rangle \langle \tilde{v} \rangle S_i'(t)\, \mathrm{d}t, \tag{2.8}$$

where T_w is the wave period, and $S_i'(t)$ is defined as

$$S_i'(t) = \begin{cases} 1, & \text{when the point } \langle \tilde{u} \rangle, \langle \tilde{v} \rangle \text{ is in the } i\text{th quadrant,} \quad (2.9a) \\ 0, & \text{otherwise.} \quad (2.9b) \end{cases}$$

$\overline{\tilde{u}\tilde{v}}_2$ and $\overline{\tilde{u}\tilde{v}}_4$ come from the second and fourth quadrants of the $\langle \tilde{u} \rangle, \langle \tilde{v} \rangle$-plane, whereas $\overline{\tilde{u}\tilde{v}}_1$ and $\overline{\tilde{u}\tilde{v}}_3$ come from the other two quadrants.

The phase-averaged turbulent stress $\langle u'v' \rangle$ was also sorted, but into two parts, according to the sign of $\langle u'v' \rangle$. Negative and positive contributions to $\overline{u'v'}$, denoted as $\overline{u'v'}_i$ and $\overline{u'v'}_2$ are such that

$$\frac{\overline{u'v'}_j}{\overline{u'v'}} = \frac{1}{\overline{u'v'}} \frac{1}{T_w} \int_0^{T_w} \langle u'v' \rangle S_j''(t)\, \mathrm{d}t \quad (j = 1, 2) \tag{2.10}$$

and $S_j''(t)$ is defined as

$$S_j''(t) = \begin{cases} 1, & \text{when } \langle u'v' \rangle < 0, \quad (2.11a) \\ 0, & \text{when } \langle u'v' \rangle > 0. \quad (2.11b) \end{cases}$$

The choice of classification of the $\langle \tilde{u}\tilde{v} \rangle$ and $\langle u'v' \rangle$ stresses according to the signs of $\langle \tilde{u} \rangle, \langle \tilde{v} \rangle$ and $\langle u'v' \rangle$ was dictated by the scheme used to deduce these stresses. For the $\langle \tilde{u}\tilde{v} \rangle$ stress, both of the phase-averaged velocities $\langle \tilde{u} \rangle$ and $\langle \tilde{v} \rangle$ were available (but not their instantaneous values $\tilde{u}, \tilde{v}$), whereas for the $\langle u'v' \rangle$ stress only the product $\langle u'v' \rangle$ was available. The latter was calculated according to the following relationship:

$$\langle u'v' \rangle \approx \langle uv \rangle - \langle u \rangle \langle v \rangle. \tag{2.12}$$

The difference $\langle u'v' \rangle - \overline{u'v'}$ represents the w.c. turbulent Reynolds stress. For comparison of our results with those obtained by other investigators, the stress $\overline{uv}$ was further classified according to the 'Hole' method, which is an extended Quadrant technique introduced by Lu & Willmarth (1973) (see also §3.6 and figure 8*a*). With this scheme, large contributions to $\overline{uv}$ from each quadrant can be extracted leaving the smaller fluctuating uv signal in the 'hole'. The contribution to $\overline{uv}$ from the 'hole' corresponds to that during the more quiescent periods. Bogard & Tiederman (1986) have recently found that this technique has a high probability of detecting the ejections and a low probability of false detections.

3. Results

3.1. *Mean velocity profiles*

Figure 1 shows mean velocity profiles in wall coordinates. A detailed discussion of the mean velocity statistics can be found in I. The lower part represents the logarithmic region of a typical turbulent-boundary-layer velocity profile, whereas the upper part

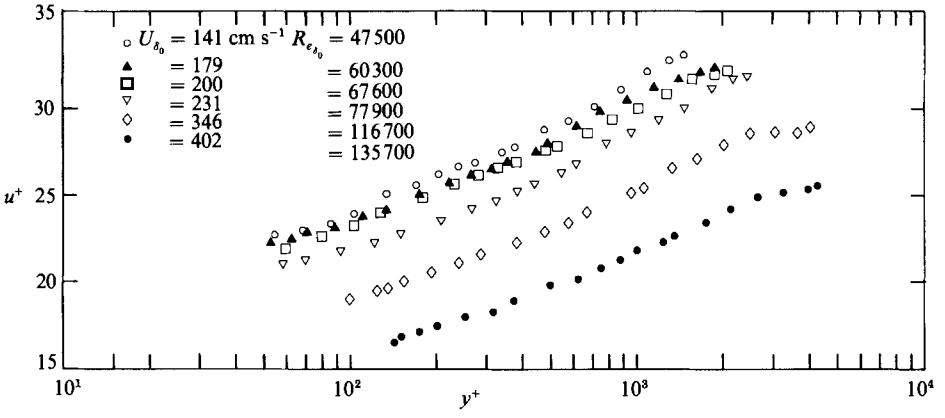

FIGURE 1. Mean velocity profiles in wall coordinates. $R_{e\delta_0} = U_{\delta_0}\delta_0/\nu$.

shows the wake characteristic. At the higher wind speeds, the wake becomes more pronounced, the elevation where it begins to be felt is lower, and the lower portion of the profile close to the air–water interface deviates from the logarithmic law. This deviation may be attributed to the generation of the surface drift current, whose magnitude is proportional to the wind speed. The wake characteristic of mean velocity profiles has also been observed by Hsu *et al.* (1981) and Hsu & Hsu (1983).

The mean velocity data were fitted to a wake log–linear expression to determine the boundary-layer thickness δ, the wake parameter $\pi(x)$, and friction velocity u_*. Then, in wall coordinates,

$$u^+ = \frac{1}{\kappa}\ln y^+ + C + \frac{\pi(x)}{\kappa}\left\{1-\cos\left(\frac{\pi y^+}{\delta^+}\right)\right\}, \tag{3.1}$$

where

$$u^+ = \frac{U-U_{\rm ds}}{u_*}; \quad y^+ = \frac{y^* u_*}{\nu}; \quad \delta^+ = \frac{\delta u_*}{\nu}; \quad C = u^+_{\delta_0} - \frac{1}{\kappa}\ln\delta^+ - \frac{2\pi(x)}{\kappa}. \tag{3.2a, b, c, d}$$

Here $\kappa(=0.4)$ is the von Kármán constant and $U_{\rm ds}$ is the (Eulerian) mean surface drift current. According to Phillips (1977), $U_{\rm ds} = U_{{\rm ds},1} - U_{{\rm ds,s}}$, where $U_{{\rm ds},1}$ and $U_{{\rm ds,s}}$ represent the Lagrangian and w.c. (i.e. Stokes) mean drift current. The latter may be taken as $(ak)^2 c$ (Kinsman 1965); $U_{{\rm ds},1}$ is usually approximated as $\approx 0.55u_*$, but the recent wave-following measurements of Cheung (1985), under similar wind and wave conditions, have shown that $U_{{\rm ds},1} \approx 0.65u_*$. Then, because in this investigation $U_{\rm ds}/u_*$ varies between 0.21 and 0.53, it represents a very small correction to the ratio U/u_* (which is $\geqslant 20.0$) and can be safely neglected in (3.2*a*). C represents the intercept of the logarithmic portion of mean velocity profiles. Its variation with wind speed (also seen in figure 1) can be ascribed to the thinning of the viscous sublayer as the wind speed increases. The latter is caused by variations in the surface roughness (see also I and Papadimitrakis *et al.* 1987).

Equation (3.1) remains valid for $y^+ \geqslant 40$–45, i.e. outside the linear sublayer and buffer zone. The former is defined as the region where $u^+ = y^+$ (i.e. $0 \leqslant y^+ \leqslant 5$–10). In hydrodynamically smooth flows, the edge of this linear profile (located at $y^+ \approx 10$) characterizes the extent of the viscous sublayer. The buffer zone represents the transitional region between the linear sublayer and the logarithmic region of mean wind profile, and extents between $5\text{–}10 \leqslant y^+ \leqslant 40\text{–}45$.

Table 1 lists the parameters U_{δ_0} (cm/s), u_* (cm/s), c/U_{δ_0}, c/u_*, C, ka, $k\delta$, ky_c^*, $k\delta_*$

U_{δ_0}	u_*	c/U_{δ_0}	c/u_*	C	ka	$k\delta$	ky_c^*	$k\delta_*$	$k\delta_m$
141	4.25	1.11	36.5	12.76	0.11	2.15	∞	0.015	∞
179	5.52	0.87	28.1	12.35	0.11	2.15	0.62	0.011	0.65
200	6.20	0.78	25.1	11.87	0.10	1.95	0.20	0.010	0.36
231	7.24	0.68	21.4	10.77	0.11	2.11	0.061	0.009	0.09
346	11.91	0.45	13.0	7.48	0.10	1.44	0.005	0.005	0.02
402	15.57	0.39	10.0	4.12	0.11	1.44	0.004	0.004	0.01

TABLE 1. Experimental conditions

and $k\delta_m$ which characterize the wind and wave conditions. The mean wind velocity U_{δ_0} was conveniently measured at the channel centreline ($y = \delta_0 = \frac{1}{2}H$); y_c^*, δ_* and δ_m represent mean critical height, and thicknesses of the viscous sublayer and nonlinear critical layer, respectively. They are given as† (Phillips 1977; Hsu & Hsu 1983)

$$y_c^* = \frac{\nu}{u_*}\exp\left\{\kappa\left(\frac{c}{u_*}-C\right)\right\}; \quad \delta_* = \frac{10\nu}{u_*}; \quad \delta_m = \left\{\frac{4\hat{v}_c}{kU_c'}\right\}^{\frac{1}{2}}, \tag{3.3a, b, c}$$

where $\hat{v}_c$ is the amplitude of the vertical w.c. velocity perturbation, as given by an inviscid solution, and $U_c' = \mathrm{d}U/\mathrm{d}y^*$, both evaluated at y_c^*. For a logarithmic mean wind profile, $\hat{v}_c$ may be approximated by (see also Benjamin 1959)

$$\hat{v}_c = \frac{ka(ky_c^*)^2 J_0 A_\infty u_*}{\kappa[1-(ky_c^*)^2\,\mathrm{e}^{(ky_c^*)}J_1]}, \tag{3.4}$$

where $$J_0(ky_c^*) = \int_1^\infty (\ln x)^2\,\mathrm{e}^{-(ky_c^*)x}\,\mathrm{d}x; \quad J_1 = \int_1^\infty (\ln x)^2\,\mathrm{e}^{-(ky_c^*)x}G(x)\,\mathrm{d}x,$$

$$G(x) = \int_x^{x_\infty}[(\ln x)^{-2}-(\ln x_\infty)^{-2}]\,\mathrm{d}x \quad \text{for } x < x_\infty,$$

$$0 \quad \text{for } x > x_\infty,$$

and $x_\infty = \exp[\kappa(U_{\delta_0}-c)/u_*]$. The coefficient A_∞ is determined from a least-squares fitting of the measured $\hat{v}$ values, in the free stream, to the expression

$$\hat{v} = A_\infty\, ka(U_{\delta_0}-c)\,\mathrm{e}^{-ky^*}.$$

It was found that A_∞ decreases with increasing wind speed and is of $O(1)$. Then substitution of (3.3*c*) into (3.4) yields

$$k\delta_m = 2[ka(ky_c^*)^3\,\Gamma J_0]^{\frac{1}{2}}; \quad \Gamma = \{1-(ky_c^*)^2\,\mathrm{e}^{(ky_c^*)}J_1\}^{-1}A_\infty. \tag{3.5a, b}$$

3.2. *Structure of the wave-coherent flow field*

We discuss here the wind and wave characteristic scales and their mutual coupling. We also discuss the lengthscales associated with the critical-layer thickness. We then examine the changes in the critical and Stokes‡ layer structures caused by turbulent diffusion and mixing, the influence of mean wind shear upon the Stokes layer and of nonlinearities on the critical layer, the interaction between the critical and Stokes layers and their influence upon the w.c. flow field. Finally we describe the structure

† This definition of δ_* may not be appropriate for non-smooth surface roughness conditions.

‡ This layer is in the air and should not be confused with the Stokes layer below the interface.

of the w.c. flow field in terms of the above scales and the behaviour of the critical and Stokes layers.

3.2.1. *Lengthscales of the wave-coherent flow field*

The wind field is characterized by the global and local lengthscales δ and δ_*. They indicate the extent of mean velocity variation, and the lower limit of turbulent mixing near the interface, respectively. The w.c. field is, in turn, characterized by a global lengthscale, the wavelength k^{-1}, and two local scales, the wave amplitude a and the (viscous) Stokes-layer thickness $\beta^{-1}[=(2\nu/\omega)^{\frac{1}{2}}=0.223$ cm], where ω is the radian wave frequency; k^{-1} indicates the extent of the w.c. flow field, whereas a and β^{-1} characterize the undulation as well as the variation of this field near the interface. The above scales form the non-dimensional parameters ka, $k\beta^{-1}$, $k\delta_*$ and $k\delta$. The w.c. flow field has different characteristics when the critical height y_c^* is comparable with either the global or local scale. Its behaviour is also different below and above y_c^*. Below y_c^*, the flow is still turbulent and behaves as if it were in an undulating channel bounded by the wavy surface and the lower boundary of the cat's eye pattern (for a description of this pattern see, for example, Phillips 1977). Above y_c^*, the w.c. flow depends strongly on the cat's eye. In this investigation, $k\beta^{-1}(\approx 0.009) \ll ka$; consequently, when turbulence diffusion is weak, the (viscous) Stokes layer is expected to be very thin and undulating along the wave surface. Furthermore, since $k\delta \approx O(1)$ and $k\delta_* \ll k\delta$, it is also expected that the w.c. perturbations $(\tilde{u}, \tilde{v})$ will be affected by both the mean wind shear and turbulence.

3.2.2. *Critical-layer effects; linear and nonlinear critical-layer behaviour*

When $c/U_{\delta_0} > 1, ky_c^* = \infty$ and the entire boundary layer is below the critical height. Our results also indicate that now $k\beta^{-1} \approx k\delta_*$. Then the upper portion of the Stokes layer is modified by turbulent diffusion and its thickness becomes comparable with the wave amplitude. As a consequence of the diffusion of the Stokes layer into the boundary layer the w.a. stress $-\overline{\tilde{u}\tilde{v}}$ oscillates with height in the water proximity. In the boundary-layer region ($0 < ky^* < k\delta$), $\tilde{u}$ and $\tilde{v}$ are also affected by the mean wind shear. However, in the free stream ($ky^* > k\delta$) they maintain a potential-flow character (see I).

When $c/U_{\delta_0} < 1$ and $ky_c^* \approx O(k\delta)$, $\tilde{u}$ and $\tilde{v}$ still exhibit a potential-flow behaviour in the free stream, and the stress $-\overline{\tilde{u}\tilde{v}}$ also shows a similar oscillatory behaviour with height in the boundary layer. Yet the magnitude of the latter changes owing to the existence of the critical layer.

The presence of this layer smooths out the discontinuity that presumably exists at y_c^* in a linear quasi-laminar analysis. In such an analysis viscosity becomes important near y_c^*. The resulting (viscous) critical layer has a finite thickness δ_c, given as $\delta_c = (\nu/kU_c')^{\frac{1}{3}}$ (Miles 1959). However, turbulent mixing may overtake viscous diffusion and produce a much thicker critical layer, as the dimensionless wave speed decreases and the critical height approaches the energetic turbulent region. The thickness of the turbulence-modified linear critical layer, δ_{ct}, may be also calculated from an expression similar to that given for δ_c, but with ν replaced by the eddy viscosity $\nu_t = \kappa u_* y^*$. Calculations of δ_{ct} and δ_c (not shown here) indicate that $\delta_{ct} \gg \delta_c$, the latter being of $O(0.02)$. When $c/U_{\delta_0} = 0.87$ (or $c/u_* \approx 28$), δ_{ct} actually becomes comparable with δ.

The nonlinearities of the wave-induced flow can also play a role in smoothing out the vorticity discontinuity at y_c^* (Davis 1969; Benney & Bergeron 1969). The significance of nonlinear effects in determining the behaviour of the w.c. flow field, as well as in enhancing the energy transfer from wind to waves, has been emphasized

by Robinson (1974) and Phillips (1977). According to Robinson (1974), nonlinear instabilities in parallel shear flows develop as a series of temporally growing spiral vortices, a description consistent with experimental observations (see also §1.1). Nonlinearities become important, relative to viscous effects, if the wave slope ka, and the Reynolds number of the flow Re (say $= u_* \delta/\nu$), satisfy simultaneously the conditions $ka \ll 1$; $Re \gg 1$ and $ka \gg Re^{-\frac{3}{4}}$ (Benney & Bergeron 1969). Since the values of Re ($= \delta^+$), shown in table 2 of I, do satisfy the above requirements we might argue that nonlinear effects become significant in this investigation. Comparison of the nonlinear critical-layer thickness δ_m with δ_{ct} also indicates that $k\delta_m \geqslant k\delta_{ct}$, the former being larger at the higher c/U_{δ_0} values. Then the results of $k\delta_c$, $k\delta_{ct}$ $k\delta_m$, and the above observation suggest that the nonlinear critical layer, plays an important (or perhaps the most important) role in determining the behaviour of the w.c. flow field, as Robinson (1974) and Hsu & Hsu (1983) also suggested. Yet the effect of turbulence on the nonlinear critical-layer structure is considerable and cannot be neglected.

3.2.3. *Mean wind and turbulence effects*

With the various critical-layer thicknesses described, we now consider the influence of mean wind shear and turbulence diffusion on the Stokes layer; we then attempt to explain the behaviour of the w.c. flow below and above y_c^*.

The effect of mean wind shear on the Stokes layer is quantified by the Tietjens function $T(-Z)$, defined conventionally in the hydrodynamic stability theory (Lin 1955). The argument $Z[= c(kU_0'/\nu)^{\frac{1}{3}}/U_0'$, where U_0' is the slope of the mean wind profile at $y^* = 0$] is the parameter that measures this mean shear effect (Benjamin 1959; Hsu & Hsu 1983). In fact, the surface friction layer behaves as if, at $y_n^* = c/U_0'$, there were a critical layer with thickness of order $\delta_n = (kU_0'/\nu)^{-\frac{1}{3}}$. Then the parameter Z represents the distance of the interface from this hypothetical critical layer, using the actual critical-layer thickness as a measure. Asymptotically, as $Z \to \infty$, the surface friction layer will reduce to the Stokes layer. For this reason we shall refer to this surface friction layer as a 'modified' Stokes layer. The latter has a thickness of $O(\beta^{-1})$, if Z is very large, and of $O(\delta_n)$ if Z is small. Since $U_0' = u_*^2/\nu$, it can be shown that $Z = R_w^{-\frac{1}{3}}(c/u_*)^{\frac{4}{3}}$, where $R_w = c/k\nu = 2(k\beta^{-1})^{-2}$ is the wave Reynolds number. For better understanding of the conditions of this investigation, the parameters $k\delta_n[= R_w^{-\frac{2}{3}}(c/u_*)^{\frac{2}{3}}]$, $ky_n[= R_w^{-1}(c/u_*)^2]$ and Z are shown in table 2 as a function of dimensionless wave speed. Since Z is not large (< 8, according to Benjamin 1959), it is expected that the influence of the mean wind shear (near the wave surface) on the Stokes layer will be considerable at all wind speeds.

We now examine the effect of turbulence diffusion on the Stokes layer and, subsequently, on the w.c. flow. Comparison of the values of $k\delta_n$ and ky_n^* with the corresponding values of $k\delta_*$ shown in table 1 indicates that the upper portion of the Stokes layer is influenced by turbulence diffusion. The parameter $\delta_*\beta[= 10(2R_w)^{-\frac{1}{2}}(c/u_*)]$, which measures the thickness of the viscous sublayer relative to the Stokes layer, also quantifies the effect of turbulence on the latter, and is listed in table 2. As seen, $\delta_*\beta$ decreases with decreasing dimensionless wave speed and, progressively, a greater portion of the Stokes layer penetrates deeper into the boundary layer. Using a simple eddy-viscosity model, it might be argued that the turbulence-modified Stokes layer has a characteristic lengthscale based on $\beta_t = [\omega/2(\nu+\nu_t)]^{\frac{1}{2}}$; $\beta_t^{-1} \gg \beta^{-1}$ and, at high dimensionless wave speeds, β_t^{-1} actually becomes comparable with the wave amplitude. If, to a first approximation, the eddy mixing is assumed to be a local process, then the effect of turbulence on the Stokes layer can be evaluated by replacing β (appearing in the viscous expressions

c/U_{δ_0}	1.10	0.87	0.78	0.68	0.45	0.39
c/u_*	36.5	28.1	25.0	21.4	13.0	10.0
$k\delta_n$	0.013	0.011	0.010	0.009	0.007	0.005
ky_n^*	0.054	0.032	0.025	0.019	0.007	0.004
Z	4.16	2.94	2.51	2.04	1.05	0.74
$\delta_*\beta$	1.64	1.27	1.13	0.99	0.59	0.45

TABLE 2. Effects of mean wind shear and turbulence on Stokes layer

of the w.c. velocities) with β_t. Such substitution results in a modified w.a. stress, which can be approximated as

$$\overline{\tilde{u}\tilde{v}}_s \approx A_0(kac)^2 \exp\left\{-ky^* + \int_0^{y^*} \beta_t \, dy^*\right\} \sin\left\{\int_0^{y^*} \beta_t \, dy^*\right\}, \tag{3.6}$$

where A_0 (≈ 1.5) is an amplification factor accounting for the effect of mean flow (see also Hsu & Hsu 1983), and the subscript s indicates contributions to the w.a. stress from the Stokes layer. Yet β_t^{-1} cannot grow indefinitely with decreasing dimensionless wave speed (being proportional to ν_t) for, as the wind speed increases and the critical layer approaches the interface, the reduced turbulence intensity in the region below the critical height (relative to its maximum value at the constant stress-layer elevation), and the vortical layer associated with the cat's eye pattern render diffusion less effective. This high-vorticity layer acts somehow as a barrier which limits the upward diffusion of the turbulent Stokes layer, but also generates additional w.a. Reynolds stresses owing to the transport of vorticity when the fluid circulates around the cat's eye. In this sense, the confined Stokes layer (by the vortical layer from above and the density interface from below) behaves as a compressed layer.

One can also interpret this compression effect of the critical layer on the turbulent Stokes layer in terms of the vortex force introduced by Lighthill (1962). The latter results from the greater disparity between the vorticity of particles and their surroundings near the critical level. The net vortex force per unit area, F_c, acting on the layer is proportional to the excess (or defect) of vorticity carried through the critical layer by the fluid, namely

$$F_c = \beta_1 \rho \frac{\pi \hat{v}_c^2}{2k}\left[\frac{-U_c''}{U_c'}\right] = \beta_1 \rho(-\overline{\tilde{u}\tilde{v}}_c), \tag{3.7a, b}$$

where ρ is the air density, $\beta_1 \approx O(1)$, and U_c'' denotes the curvature of mean wind profile at the critical height; $-\overline{\tilde{u}\tilde{v}}_c$ represents the w.a. stress produced by the critical layer. When the critical layer falls inside the logarithmic region of the mean velocity profile (i.e. when $ky_c^* \approx O(k\delta)$ or less), $U_c''/U_c' \propto (ky_c^*)^{-1}$, and $\hat{v}_c$ (given by (3.4)) is small; consequently, F_c is also small. Therefore, in the region below y_c^* the compression of the turbulent Stokes layer by the vortex force (between the vortical layer from above and the waveform from below) is weak, and the w.c. flow field may be represented by the superposition of the flow fields induced by the two layers. The distribution of the total w.a. stress $-\overline{\tilde{u}\tilde{v}}$ is then described by the sum of $-\overline{\tilde{u}\tilde{v}}_s$ and $-\overline{\tilde{u}\tilde{v}}_c$.

When c/U_{δ_0} is low, so that $ky_c^* < ka$ and U_c'' remains negative, the w.c. perturbations near the interface depend mainly on: (i) the compression of the flow field below y_c^* by the vortex force, and (ii) the interface boundary condition. Then the critical layer becomes thin and undulates with the waveform. Below y_c^*, $\tilde{u}$ and $\tilde{v}$ are determined by the critical layer alone. Although $\hat{v}_c$ decreases with decreasing c/U_{δ_0}, it can be

shown that, in this regime, F_c actually increases with decreasing dimensionless wave speed; consequently, F_c becomes larger and the compression of the w.c. flow field by the vortex force is now stronger. Yet the mean stress associated with the turbulence-modified Stokes layer, $-\overline{\tilde{u}\tilde{v}}_s$, decreases as the wind speed increases (for β_t decreases). It can also be shown that for $c/U_{\delta_0} > 0.45$, this stress is $> -\overline{\tilde{u}\tilde{v}}_c$. Then, depending on the relative magnitude of $-\overline{\tilde{u}\tilde{v}}_s$ compared with $-\overline{\tilde{u}\tilde{v}}_c$, the total w.a. stress below ky_c^* may decrease or increase as c/U_{δ_0} decreases. Our measurements indicate that the total w.a. stress, at the lowest point of measurements, decreases with decreasing c/U_{δ_0} (except when $c/U_{\delta_0} = 0.68$ or $c/u_* = 21.4$). Above y_c^*, $\tilde{u}$ and $\tilde{v}$ depend on the undulations of the upper boundary of the cat's eye pattern, defined by

$$\tilde{y}_m^* = \delta_m \cos\tfrac{1}{2}(kx^* - \omega t + \theta_c), \tag{3.8}$$

where θ_c is the phase angle locating the centre of the cat's eye (Phillips 1977).

If c/U_{δ_0} is further decreased so that $ky_c^* \ll ka, U_c''$ will eventually become positive (when y_c^* falls inside the lower portion of the buffer zone). Then $-\overline{\tilde{u}\tilde{v}}_c$ will become negative, since this stress is proportional to $-U_c''$, and the vortex force will be directed upwards, thereby reducing the compression of Stokes layer and (perhaps) rendering turbulence diffusion more effective again.

It should be pointed out that at low c/U_{δ_0} values the measured w.a. stress is greater than the sum of $-\overline{\tilde{u}\tilde{v}}_s$ and $-\overline{\tilde{u}\tilde{v}}_c$. Then, since at $c/U_{\delta_0} = 0.45$ and 0.39 $-\overline{\tilde{u}\tilde{v}}$ remains negative, it might be argued that the actual critical-layer contribution to the total w.a. stress is larger than the Miles (1957) theory predicts.

In summary, the structure of the w.c. velocity field is very sensitive to the height of the critical layer. As the dimensionless wave speed decreases from $c/U_{\delta_0} = 0.87$ to 0.68, the critical height decreases rapidly from $ky_c^* = 0.62$ to 0.061 while the global lengthscale of the wind field, δ, remains practically unchanged. The viscous sublayer becomes progressively thinner (being inversely proportional to u_*) and a greater portion of the upper part of the Stokes layer is influenced by turbulent diffusion. As the critical height decreases, the cat's eye (confined from below by the density interface) becomes slender, undulating along the waveform, and more uneven on the upper and lower side of the critical layer since $ky_c^* < k\delta_m$. The compression of the w.c. flow field below the critical height may enhance the production of the w.a. stress in the critical layer (i.e. the stress $-\overline{\tilde{u}\tilde{v}}_c$).

When c/U_{δ_0} is further decreased so that $ky_c^* < k\delta_m \ll ka$, the critical layer and the region below the critical height are very thin and the behaviour of the w.c. flow is mainly determined by the critical layer.

3.2.4. *Low- and high-critical-level regimes*

From table 1 we find that $k\delta_m > ka$ only when $c/U_{\delta_0} \geqslant 0.68$. Apparently, there exists a critical value of c/U_{δ_0} ($= \mu_c$) which distinguishes the flow regimes of low and high critical level. These two regimes are associated with strong and weak (zero for $c/U_{\delta_0} \geqslant 1.0$) compression of the w.c. flow field below y_c^* resulting, respectively, in a significant and weak suppression of the w.a. stress production. The flow regime of low critical level seems to be also signified by: (i) a phase jump of approximately 180° in the profiles, $\theta_{\tilde{r}_{12}}$, of the w.c. Reynolds stress phase lags (with respect to the surface wave); and (ii) a small positive phase lag $\theta_{\tilde{u}}$ (i.e. $0° < \theta_{\tilde{u}} \ll 90°$) in the corresponding profiles of the w.c. velocity $\tilde{u}$, close to the water surface.† Our observations suggest that μ_c may be located at somewhere near $c/U_{\delta_0} \approx 0.68$, when $k\delta_m \approx ka$. The results

† For an explanation of this $\theta_{\tilde{r}_{12}}$ and $\theta_{\tilde{u}}$ at $c/U_{\delta_0} = 0.55$, 0.45 and 0.39 see I.

of Hsu & Hsu (1983) also show that $k\delta_m \approx ka$, when $0.65 < c/U_{\delta_0} < 0.74$. Furthermore, (3.5) indicates that $k\delta_m \approx f(ka, ky_c^*, c/u_*)$. Since y_c^* depends on both the properties of the mean wind profile and the wave characteristics, and ka depends also on fetch (Huang, Long & Bliven 1981; Hsu *et al.* 1982), we conclude that μ_c is not a universal constant but may depend on fetch and possibly on the boundary-layer development (artificial versus natural; wave tank versus open sea).

As seen from table 2, for $c/U_{\delta_0} \gtrless 0.68$ (or $c/u_* \gtrless 21.4$), $ky_n^* \gtrless k\beta^{-1}$, indicating that perhaps there is another critical $(c/u_*)_{cr}$ ratio associated with the high- and low-critical-level regimes. Its value can be determined from the condition: $ky_n^* \approx k\beta^{-1}$, and is given by $(c/u_*)_{cr} = (2R_w)^{\frac{1}{4}}$. For the present experiments $(c/u_*)_{cr} \approx 20$. This critical ratio closely approximates the value of c/u_* that corresponds to μ_c. The latter observation may facilitate the selection of the appropriate value of c/u_* resulting from the condition $k\delta_m \approx ka$, if this equation has multiple roots with respect to c/u_*.

3.2.5. *Zone of significant wave-associated stresses*

When $c/U_{\delta_0} \gtrsim 0.68$ (or $c/u_* > 20$), turbulence diffusion and mixing reduce the decay rate,

$$D = -ky^* + \int_0^{y^*} \beta_t \, dy^*,$$

of the w.a. stress with height and augment the width (ky_0^*) of the zone where $-\overline{\tilde{u}\tilde{v}}$ remains significant, as c/u_* increases. The reduction of D with decreasing wind speed results from the growth of β_t. When $c/U_{\delta_0} < 0.68$ (or $c/u_* < 20$), turbulence diffusion becomes less effective (for both β_t decreases and the cat's eye vortical layer, located now closer to the water surface, prevents the Stokes layer from spreading upwards). Then, owing to the reduced influence of turbulence diffusion and mixing on D beyond δ_m, the width ky_0^* is expected to decrease as δ_m becomes smaller with decreasing c/U_{δ_0}. The variation of ky_0^* with the wind and wave parameters is important for explaining the behaviour of both the distribution of the fractional contributions $\overline{uv}_i/\overline{uv}$, and the contribution of the w.a. stress to the production of the total Reynolds stress across the boundary layer. The discussion in the remaining part of this subsection is, therefore, devoted to shedding some light on this.

The width ky_0^* can be determined from the first and/or second zero crossing of the $-\overline{\tilde{u}\tilde{v}}$ stress along ky^*, that is, from the condition

$$\sin\left\{\int_0^{y^*} \beta_t \, dy^*\right\} = \sin(n\pi) \quad (n = 1, 2) \tag{3.9}$$

as the subsequent extrema of this stress decrease rapidly with increasing ky^*. This location is approximately given by

$$ky_0^* \approx \left[n\pi(\tfrac{1}{2}\kappa)^{\frac{1}{2}} + 1.90(\kappa R_w)^{-\frac{1}{2}}\left(\frac{c}{u_*}\right)\right]^2\left(\frac{c}{u_*}\right)^{-1} - (\kappa R_w)^{-1}\left(\frac{c}{u_*}\right) \quad (n = 1, 2), \tag{3.10}$$

assuming that ν_t varies as (see Cebeci & Bradshaw 1977; Street 1979; Kitaigorodskii & Donelan 1984)

$$\frac{\nu_t}{\nu} = \begin{cases} (y^+/10)^3, & 0 < y^+ \leqslant 10, & (3.11a) \\ (y^+/10)^2, & 10 < y^+ \leqslant 40, & (3.11b) \\ \kappa y^+, & 40 < y^+ \leqslant 0.2\delta^+, & (3.11c) \\ \alpha_1 \delta^+ \gamma^{-1}, & 0.2\delta^+ < y^+ \leqslant \delta^+, & (3.11d) \end{cases}$$

where $$\gamma = \frac{1}{2}\left\{1 - \mathrm{erf}\left[5\left(\frac{y^+}{\delta^+} - 0.78\right)\right]\right\}$$

is the intermittency factor and $\alpha_1 (\approx 0.07)$ is a numerical constant. Equation (3.10) is not valid when $ky_0^* > 0.2k\delta$. Owing to the eddy-viscosity approximation in the region $ky^* > 0.2k\delta$, the corresponding expression becomes more complicated. Equations (3.11*a*, *b*) have been derived from dynamic considerations in similar flows (Street 1979, p. 891), whereas (3.11*c*) is based on purely dimensional arguments. It is, therefore, valid in the logarithmic region of the boundary layer irrespective of flow type. Equation (3.11*d*) represents, however, an empirical expression derived from flat-plate boundary layers and its validity in interface flows remains to be seen.

For $c/U_{\delta_0} = 1.11, c/u_* = 36.5$ and, for $n = 1, ky_0^* \approx 0.11$ (or $y_0^*/\delta_0 \approx 0.05$). At this dimensionless wave speed, the measured $-\overline{\tilde{u}\tilde{v}}$ stress decays rapidly with height, in the water proximity, and at $ky^* \approx 0.11$ is about an order of magnitude smaller than its value at the lowest point of measurements (Papadimitrakis 1982). In the region $0.11 < ky^* < 0.2$, $-\overline{\tilde{u}\tilde{v}}$ oscillates slightly with height and then decays rapidly to zero as ky^* increases.

An expression nearly identical to (3.10) can also be derived by using the theoretical model for an oscillating turbulent boundary layer described by R. E. Davis in an Appendix to Hsu & Hsu (1983). Davis' equations (A 1)–(A 5), with $\nu_t = \nu\kappa y^+$ applied down to $y^* = 0$, lead to the expression

$$ky_0^* \approx \tfrac{1}{2}\kappa(n\pi)^2\left(\frac{c}{u_*}\right)^{-1} + n\pi(2R_{\mathrm{w}}^{-1})^{\frac{1}{2}} \quad (n = 1, 2) \tag{3.12}$$

The above relation yields $ky_0^* \approx 0.082$ for $c/u_* = 36.5$ and $n = 1$. The difference between this ky_0^* value and 0.11 may be attributed to the dissimilar eddy viscosity approximations used in the buffer and linear sublayers. When $c/U_{\delta_0} < 0.68$, (or $c/u_* < 20$), ky_0^* can still be determined from (3.9) and, assuming that for $y^+ \geqslant \delta_{\mathrm{m}}^+$: $\nu_t \approx \kappa\delta_{\mathrm{m}}^+$, is given by

$$ky_0^* \approx \left[\left(\frac{c}{u_*}\right)^2 R_{\mathrm{w}}^{-2} + \kappa(k\delta_{\mathrm{m}})\left(\frac{c}{u_*}\right)R_{\mathrm{w}}^{-1}\right]^{\frac{1}{2}}\left[700n\left(\frac{c}{u_*}\right)^{-1} - 11.46\right] - \left[k\delta_{\mathrm{m}} + 2\kappa^{-1}\left(\frac{c}{u_*}\right)R_{\mathrm{w}}^{-1}\right] \quad (n = 1, 2). \tag{3.13}$$

Table 3 shows the variation of ky_0^* with c/u_* (and c/U_{δ_0}) according to (3.10)–(3.13). For $15.6 \leqslant c/u_* \leqslant 36.5$ (or $0.55 \leqslant c/U_{\delta_0} \leqslant 1.1$), the measured $-\overline{\tilde{u}\tilde{v}}$ stresses do oscillate with ky^* taking on positive and negative values, and the position of first and second zero crossing appears to reasonably agree with the above results (see also I).

At $c/u_* \approx 13.0$ and 10.0 (or $c/U_{\delta_0} \approx 0.45$ and 0.39), the w.a. stresses were found to remain negative at all measurement heights.† However, at $ky^* \approx 0.46$ and 0.40 they are about an order of magnitude smaller than their corresponding absolute maximum values. The negative sign of the w.a. stresses in the water proximity can be justified by considering the critical-layer contribution to the w.a. stresses. At these dimensionless wave speeds, $y_{\mathrm{c}}^+ \approx 11.5$ and 10.5, and U_{c}'' apparently becomes negative. Then, simple calculations show that the critical-layer contribution to $-\overline{\tilde{u}\tilde{v}}$ (i.e. the stress $-\overline{\tilde{u}\tilde{v}}_{\mathrm{c}}$) is greater than its Stokes-layer counterpart (i.e. $-\overline{\tilde{u}\tilde{v}}_{\mathrm{s}}$). Hence it is expected that, close to the water surface, $-\overline{\tilde{u}\tilde{v}}$ will remain negative. Since now $-\overline{\tilde{u}\tilde{v}}_{\mathrm{c}}$

† Inside the linear sublayer the w.a. stress should become positive again, since there $U'' = 0$ and $\overline{\tilde{u}\tilde{v}}_{\mathrm{c}} = 0$.

c/U_{δ_0}	1.10	0.87	0.78	0.68	0.55	0.45	0.39
c/u_*	36.5	28.1	25.0	21.4	15.6	13.0	10.0
$n = 1$; ky_0^*	0.11	0.14	0.15	0.16	0.14	0.13	0.10
$n = 2$; ky_0^*	0.33	0.40	0.43	0.51	0.48	0.46	0.40

TABLE 3. Variation of ky_0^* with wind and wave conditions

dominates the total w.a. stress, (3.13) may no longer be valid and the corresponding values of ky_0^* shown in table 3 for $n = 1$ may become questionable. However, because the vortex force is directed upwards and renders turbulent diffusion more effective again, it might be argued that the actual width ky_0^* will be larger than its values shown in table 3 for $c/U_{\delta_0} = 0.45$ and 0.39. The significance of this observation will become apparent in the next section where we discuss the behaviour of correlation coefficient(s) with height and dimensionless wave speed.

3.3. *Correlation coefficients*

Figure 2 shows the distribution of the correlation coefficients R and R'

$$R = -\frac{\overline{uv}}{\{[\overline{u^2}][\overline{v^2}]\}^{\frac{1}{2}}}; \quad R' = -\frac{\overline{u'v'}}{\{[\overline{u'^2}][\overline{v'^2}]\}^{\frac{1}{2}}}. \tag{3.14a, b}$$

As can be seen, the turbulent correlation coefficient R' is nearly constant in most of the equilibrium region† (i.e. $0.14k\delta \leqslant y^*/\delta_0 \leqslant 0.28k\delta$ or $0.3k\delta \leqslant ky^* \leqslant 0.6k\delta$) and assumes a mean value R'_{m} which decreases from about 0.39 to 0.30, as c/U_{δ_0} increases from 0.39 to 1.11. Close to the water surface (i.e. $y^*/\delta_0 < 0.14k\delta$ or $ky^* < 0.30k\delta$) R' increases, whereas in the free stream (i.e. $y^*/\delta_0 > 0.28k\delta$ or $ky^* > 0.6k\delta$) it decreases monotonically as y^*/δ_0 increases. Lu & Willmarth (1973) have reported a value of $R' = 0.44$, and values as large as 0.5 have been measured by other investigators (Wallace *et al.* 1972; Nakagawa & Nesu 1977, 1981). Our lower R' values, throughout the boundary layer and the water proximity in particular, compared to wall-bounded and open-channel flow data, are thought to be the physical consequence of turbulence alteration through: (i) the interaction with the large-scale velocity perturbations induced by the mechanically generated waves; and (ii) the generation of the wind-induced drift current. The latter effect results in a reduction of both the air friction velocity u_*, and the mean turbulent shear and normal Reynolds stresses, relative to their values over a solid surface. The fact that the equilibrium-layer correlation coefficient R'_{m} decreases as c/U_{δ_0} increases may be partly attributed to variations of the surface roughness condition from transitionally rough to smooth (based on traditional measures), although the data of Ligrani & Moffat (1986) over a solid-wall boundary layer indicate that such variations do not alter either the trend or the magnitude of R'. Otherwise, the comparison with previous data in pipe, wall-boundary-layer, and open-channel flows indicates that the turbulence correlation coefficient displays universal characteristics, independent of flow type and surface roughness condition.

The distribution of the correlation coefficient R shows a behaviour that is similar to that of R' only in the equilibrium and free-stream regions, as close to the water surface R either decreases or increases with non-dimensional height, depending on

† In this region a dynamic equilibrium exists between turbulence production and dissipation, and a similarity in turbulent structure is expected to be found, independent of boundary conditions.

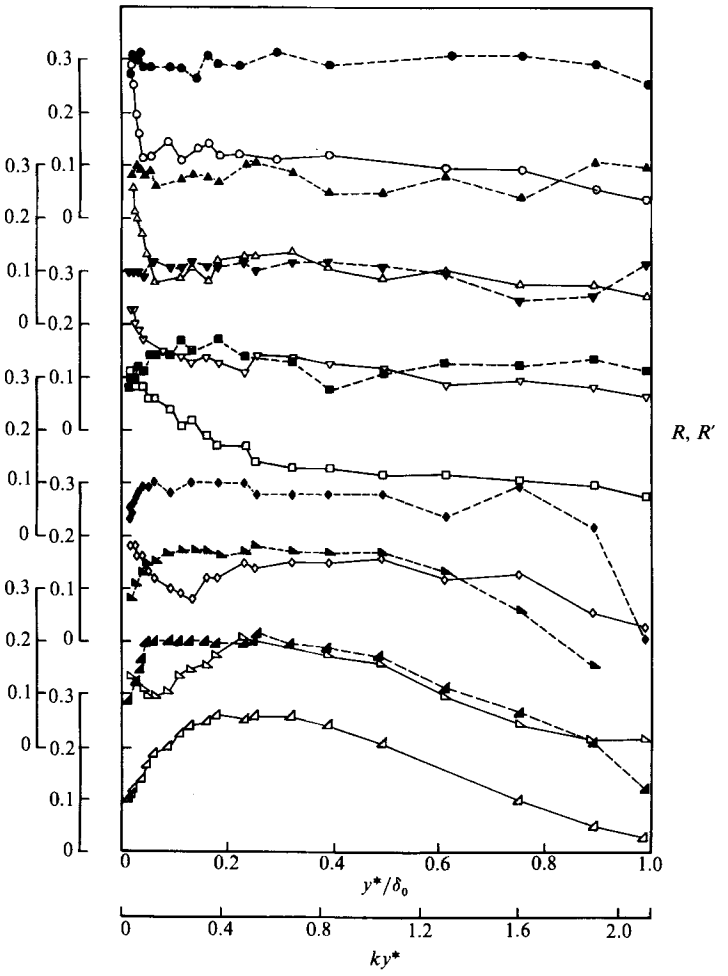

FIGURE 2. Distributions of total (R), and turbulent (R') correlation coefficients throughout the boundary layer. Open symbols denote R: ○, △, ▽, □, ◇, ◺, ◿ correspond to $c/U_{\delta_0} = 1.11$, 0.87, 0.78, 0.68, 0.55, 0.45 and 0.39. Solid symbols denote R': ●, ▲, ▼, ■, ◆, ◣, ◢ correspond to $c/U_{\delta_0} = 1.11$, 0.87, 0.78, 0.68. 0.55, 0.45 and 0.39.

c/U_{δ_0}. The mean values of R in the equilibrium region, like R'_{m}, also decrease from about 0.25 to 0.12, as c/U_{δ_0} increases from 0.39 to 1.11. Since the correlation coefficient R is directly linked to the quantitative behaviour of the fractional contributions $\overline{uv}_i/\overline{uv}\,(i = 1, \ldots, 4)$ and is mainly responsible for it (see §3.4), it is important to understand the physical mechanisms governing its variation throughout the boundary layer, under the conditions examined. A description of these mechanisms follows.

The behaviour of the correlation coefficient R in the water proximity possibly reflects the influence of the w.c. velocity perturbations $(\tilde{u}, \tilde{v})$ on the wind turbulence and their mutual interactions, as can be seen by expressing R in terms of the w.c. and turbulent stresses, namely

$$R = -\frac{\overline{\tilde{u}\tilde{v}} + \overline{u'v'}}{\{(\overline{\tilde{u}^2} + \overline{u'^2})\,(\overline{\tilde{v}^2} + \overline{v'^2})\}^{\frac{1}{2}}}. \tag{3.15}$$

The organized–random velocity component interactions result in modifications of the corresponding velocity fields. Such manifestations of wind turbulence alterations by the waves can also be found in the ratios $-\overline{u'v'}/\overline{q'^2}$, $\sigma_u = (\overline{u'^2})^{\frac{1}{2}}/u_*$, and $\sigma_v = (\overline{v'^2})^{\frac{1}{2}}/u_*$, where $\overline{q'^2}$ represents mean turbulence intensity. In the constant-stress-layer region of a typical boundary layer over a flat wall, under neutral conditions, these ratios have values of about 0.15, 2.5 and 1.3 (see, for example, Bradshaw 1978). Over sea, various investigators have reported values of σ_u, σ_v in the range $1.7 \leqslant \sigma_u \leqslant 2.3$ and $1.3 \leqslant \sigma_v \leqslant 1.6$, but there is suspicion that these values contain (unremoved) w.c. contributions (Busch 1973). In the present experiments they were found to be smaller, increasing monotonically between 0.08–0.14, 1.95–2.35 and 0.65–0.95, respectively, as c/U_{δ_0} decreases. The smaller values of these ratios and of the turbulence correlation coefficient R' as well, signify that $-\overline{u'v'}/u_*^2$ is also reduced in the presence of waves. According to I, in the constant-flux-layer region $-\overline{u'v'}/u_*^2 < 1$ (approaching unity as the wind speed increases), whereas for a flat-wall boundary layer $-\overline{u'v'}/u_*^2 \approx 1$. The behaviour of wind turbulence in the presence of waves is dependent on the ratio c/U_{δ_0} (i.e. on the critical layer), because it is affected by wave-induced modifications of the burst/sweep statistics, which are introduced through the effects of the flow in the vicinity of the critical layer on the turbulence above and below it. Again, as the wind speed increases the water wave behaves as a rigid (wavy) surface (for, as $c \to 0$: $U_{\delta_0}/c \to \infty$) and the turbulence characteristics return to their conventional flat-wall boundary-layer counterparts, although somewhat modified to account for the extra strain rates introduced by the wavy surface (see, for example, Kendall 1970).

As seen from figure 2, the zone of influence of the surface waves on R appears first to become wider as c/U_{δ_0} decreases from 1.11 to about 0.68, then (slowly) thinner as c/U_{δ_0} further decreases to 0.39, and is confined in the region $ky^* < 0.10$–0.55. This behaviour is consistent with the fact that for $c/U_{\delta_0} < 1$, $\tilde{u}$ and $\tilde{v}$ decay faster with ky^* than for $c/U_{\delta_0} > 1$. When $c/U_{\delta_0} = 1.11$, the w.c. flow is only affected by viscosity at the interface and turbulent mixing in the boundary layer, since the critical-layer effect is negligible. Then, close to the water surface $\overline{\tilde{u}^2} \approx O(\overline{u'^2})$, $\overline{\tilde{v}^2} \gg \overline{v'^2}$, $-\overline{\tilde{u}\tilde{v}} \gg -\overline{u'v'}$ and, thus, it is reasonable to assume that there the behaviour of R with height (at any given ratio c/U_{δ_0}) is dominated by the w.a. stress distribution.

For $c/U_{\delta_0} < 1$, the behaviour of R with height depends also on the distribution of $\overline{\tilde{u}^2}$ and $\overline{\tilde{v}^2}$ across the layer. Our results (see I) indicate that, in the region $0.3 < ky^* < 0.55$, $\overline{\tilde{u}^2}$ decays almost as fast as $-\overline{\tilde{u}\tilde{v}}$, being one to two orders of magnitude smaller than its maximum value at the lowest point of measurements; $\overline{\tilde{v}^2}$ decays with height more slowly than both $\overline{\tilde{u}^2}$ and $-\overline{\tilde{u}\tilde{v}}$. As c/U_{δ_0} decreases from 1.11 to 0.39 (for any fixed y^*), $\overline{\tilde{u}^2}$ increases and eventually becomes of $O(\overline{u'^2})$, whereas $\overline{\tilde{v}^2}$ decreases and, at the highest wind speed it becomes an order of magnitude smaller than $\overline{v'^2}$; $\overline{u'^2}$, $\overline{v'^2}$ and $-\overline{u'v'}$ also decay with height, but more slowly than $\overline{\tilde{u}^2}$, $\overline{\tilde{v}^2}$ and $-\overline{\tilde{u}\tilde{v}}$, respectively. At high wind speeds (say $c/U_{\delta_0} \leqslant 0.4$), the critical-layer height becomes very small and, as mentioned before, the water surface behaves approximately as a rigid (wavy) boundary. Under these conditions, the wave's influence on R gradually decreases as the wind speed increases and the trend of R with height in the water proximity becomes asymptotically similar to that over a solid (wavy) surface. Such variations should, therefore, be confined in the inner region of the boundary layer (i.e. $ky^* < 0.2k\delta$). The data of table 1 indicate that, for $c/U_{\delta_0} = 0.45$ and 0.39, $0.2k\delta = 0.39$ and 0.29, respectively. These values are smaller than their experimental counterparts (0.55 and 0.40), as shown in figure 2. This discrepancy may be partly attributed to the mobility of the interface and the continually changing surface

roughness caused by the short wavelets riding on the dominant wave with phase velocities c_s such that $c_s/u_* \approx O(1)$ or less. It can also be interpreted in terms of the critical-layer behaviour which then augments the width of the zone of influence of the w.a. stress and, consequently, enhances the influence of surface waves on R.

Figures 8 and 9 of I also show that all significant variations of the ratio $R_s = \overline{\tilde{u}\tilde{v}}/\overline{u'v'}$ occur in the region $0 < ky^* < 0.1$–0.55 where $\max R_s \approx O(1)$. Therefore, it can be argued that the variation of R across the surface layer is largely determined by the corresponding $-\overline{\tilde{u}\tilde{v}}$ stress distribution, when 0.55–$0.68 < c/U_{\delta_0} < 1.1$, and to a lesser extent when $0.39 < c/U_{\delta_0} < 0.55$–$0.68$.

3.4. *Contributions to the mean Reynolds stress from different events*

Figure 3 shows the fractional contributions $\overline{uv}_i/\overline{uv}$ to the mean Reynolds stress $\overline{uv}$, at the lowest point of measurements, as a function of dimensionless wave speed. It is seen that ejections are the largest contributor to $\overline{uv}$, with sweeps the second largest. However, the contributions from outward and wallward interactions are also significant. For $c/U_{\delta_0} \geqslant 0.68$, ejections contribute on the average 90% of the total mean stress. This fractional contribution is somewhat greater than the value 80% or 77% reported by Kim *et al.* (1971) and Lu & Willmarth (1973) for smooth, flat-wall boundary layers. In the same range of dimensionless wave speeds, sweeps contribute about 77% of the mean stress, and both first and third quadrants have identical contributions (-34% and -33%, respectively). Lu & Willmarth (1973) have reported values of 55% and -32% for the contribution of sweeps, wallward and outward interactions. Takeuchi *et al.* (1977) reported that ejections and sweeps each provide about 100% of the mean turbulent Reynolds stress, whereas wallward and outward interactions each provide -50%. Increased sweep contributions were also observed by Nakagawa & Nesu (1977) in their rough-bed, open-channel flow measurements, and were attributed to the bed roughness. For $c/U_{\delta_0} < 0.68$, a significant change in the behaviour of fractional contributions $\overline{uv}_i/\overline{uv}$ is observed. The contributions of all quadrants progressively increase. Values as high as 192%, 174%, -146% and -120% were found at $c/U_{\delta_0} = 0.39$. However, the value of the ratios $\overline{uv}_2/\overline{uv}_4$ and $\overline{uv}_1/\overline{uv}_3$ remains almost unaltered.

Both Lu & Willmarth (1973) and Nakagawa & Nesu (1977) found good agreement between measurements of the fractional contributions $\overline{uv}_i/\overline{uv}$ and their prediction throughout the boundary layer, except close to the wall and in the outer intermittent region. The predictions were made by applying either the cumulant-discard method to the Gram–Charlier probability distribution of u- and v-signals, or the assumption of joint normality for these two signals. Takeuchi *et al.* (1977) has also found that both of the turbulent fluctuations u' and v' have a remarkably Gaussian behaviour, at least up to three times their standard deviation, and that the probability density of $u'v'$ shows a distinctly non-Gaussian distribution, sensibly in agreement with the measurements of Lu & Willmarth (1973) and Nakagawa & Nesu (1977). We might, therefore, anticipate that similar or extended methods can be used to predict the various aspects of the bursting cycle in flows above an air–water interface. This conclusion will become obvious after we delineate the similarities and differences among some other relevant quantities for interface flows, conventional wall boundary layers, and open-channel flows.

Following Lu & Willmarth (1972) and Nakagawa & Nesu (1977) we have derived expressions that can be used to predict the fractional contributions $\overline{uv}_i/\overline{uv}$ at $H = 0$ (zero 'hole' size), in terms of the correlation coefficient R. These expressions

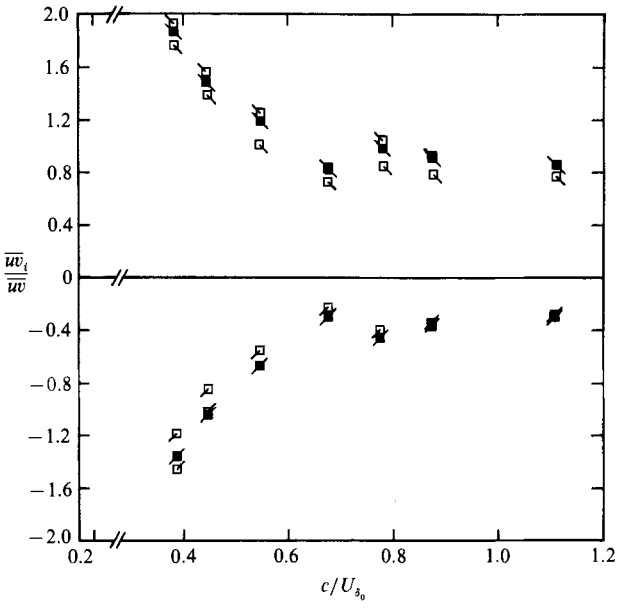

FIGURE 3. Fractional contributions to $\overline{uv}$ of the various events of the bursting cycle, at the lowest point of measurements. ◰, 1st quadrant; ◱, 2nd quadrant; ◲, 3rd quadrant; ◳, 4th quadrant. Measurement levels for respective c/U_{δ_0}: $y^*/\delta_0 = 0.018$; 0.015; 0.019; 0.015; 0.014; 0.019; 0.015. Solid symbols indicate predictions of the corresponding contributions.

are based on the assumption of joint normality of the u and v signals. In the water proximity, the ratios $\overline{uv}_2/\overline{uv}_4$ and $\overline{uv}_1/\overline{uv}_3$ have values, independent of dimensionless wave speed, of about 1.15 and 1.10, being smaller than their counterpart values over wall-bounded flows (i.e. 1.85 and 1.25). Such low values imply that the assumption of joint normality of u and v is probably better justified for interface than for smooth flat-wall flows. This assumption is indeed consistent with the measured probability densities of u', v' and $u'v'$ by Takeuchi *et al.* (1977), under similar wind and wave conditions. The effects of deviation of u and v probability density distributions from a Gaussian behaviour on the burst fractional contributions are also included in our analysis. They are usually described by the skewness and turbulence diffusion factors $S_{u,v}$ and $D_{u,v}$, where $S_u = \overline{\hat{u}^3}$, $S_v = \overline{\hat{v}^3}$, $D_u = \overline{\hat{u}\hat{v}^2}$, $D_v = \overline{\hat{v}\hat{u}^2}$ and $\hat{u} = u/(\overline{u^2})^{\frac{1}{2}}$, $\hat{v} = v/(\overline{v^2})^{\frac{1}{2}}$. Then, the ejection fractional contribution is given by the following equation:

$$\frac{\overline{uv}_2}{\overline{uv}} = \frac{(1-R^2)^{\frac{1}{2}} + R\cos^{-1}(-R)}{2\pi R} + \frac{D^-}{2(2\pi)^{\frac{1}{2}}R} + \frac{S^-}{6(2\pi)^{\frac{1}{2}}}, \tag{3.16}$$

and similar expressions hold for the other contributions; here $S^- = \frac{1}{2}(S_v - S_u)$ and $D^- = \frac{1}{2}(D_v - D_u)$. Since the organized velocity perturbations do not contribute to the skewness and diffusion factors, it follows that $S_u \approx S_{u'}$; $S_v \approx S_{v'}$; $D_u \approx D_{u'}$; and $D_v \approx D_{v'}$. The measurements of Takeuchi *et al.* (1977) and Nakagawa & Nesu (1977) have shown that, for small y^*/δ_0 (or ky^*), $S_{v'} \approx -S_{u'} \approx 0.1$–$0.2$; $D_{v'} \approx -D_{u'} \approx 0.1$–$0.2$; therefore, $S^- \approx S_{v'}$; $D^- \approx D_{v'}$. They have also observed that S^- and D^- slowly decrease with increasing surface roughness and/or wind speed. Then, comparison of the various terms on the right-hand side of (3.16) reveals that, for the range of dimensionless wave speeds considered in this investigation, the contribution

of the last two terms to $\overline{uv}_i/\overline{uv}$ is rather small (being $< 10\%$) and can be neglected. Under these conditions, the following simplified expressions for $\overline{uv}_i/\overline{uv}$ hold:

$$\frac{\overline{uv}_2}{\overline{uv}} = \frac{\overline{uv}_4}{\overline{uv}} = \frac{(1-R^2)^{\frac{1}{2}} + R\cos^{-1}(-R)}{2\pi R}, \tag{3.17}$$

$$\frac{\overline{uv}_1}{\overline{uv}} = \frac{\overline{uv}_3}{\overline{uv}} = \tfrac{1}{2} - \frac{\overline{uv}_2}{\overline{uv}}. \tag{3.18}$$

The predicted contributions $\overline{uv}_i/\overline{uv}$, according to (3.17) and (3.18) are also shown in figure 3. The agreement is very good, providing further confidence in the assumptions. Since both D^- and S^- are small and positive their net effect on $\overline{uv}_{2,4}/\overline{uv}$ is to slightly increase $\overline{uv}_2/\overline{uv}$ and/or decrease $\overline{uv}_4/\overline{uv}$, relative to their values given by (3.17) and (3.18), bringing the predicted contributions even closer to their experimental counterparts. Similar arguments also hold for the interaction contributions.

The dependence of the fractional contributions $\overline{uv}_i/\overline{uv}$ on c/U_{δ_0} (or c/u_*) has also been observed by Chambers & Antonia (1981). However, their results show that these contributions increase as c/u_* becomes large (≈ 81), a behaviour consistent with the decreasing values of coefficient R found in the open sea as c/u_* increases (Volkov 1970). Such field dependence of both $\overline{uv}_i/\overline{uv}$ and R on c/u_* appears to be at odds with our measurements. Since Volkov's (1970) data were collected at a height $y = 2$ m from the mean water level, in the presence of a swell and under unstable conditions, it is possible that their non-dimensional height, ky^*, falls in the region where R remains nearly constant (for a fixed c/u_*), assuming that the observed laboratory behaviour of R with height for $21 < c/u_* < 37$ can also be found in the ocean at large values of c/u_*. Therefore, the field trend of decreasing R with c/u_* is not inconsistent with our measurements (figure 2). For $10 < c/u_* < 40$, Volkov's (1970) data indicate somewhat higher R-values than our measurements, but this can probably be attributed to the unstable stratification.† Because the measurement height in Chambers & Antonia (1981) ($y = 5$ m) corresponds to $ky^* \approx 0.3$ and their data were collected under more unstable conditions ($Ri \approx -0.43$) than those corresponding to Volkov's (1970) experiments ($Ri \approx -0.025$), it is expected that their R-value at $c/u_* = 81$ will be greater than 0.05, as suggested by Volkov (1970), and possibly about 0.10–0.12. Here Ri represents the gradient Richardson number. Such a correlation coefficient, however, corresponds (according to (3.17) and (3.18)) to fractional contributions $\overline{uv}_i/\overline{uv}$ nearly equal to the results shown in figure 3, for $c/U_{\delta_0} \approx 0.55$. The critical layer in their run with $c/u_* = 81$ was found to be located at about 49 m from the mean water level and, since $ky_c^* \approx 3.3$, it is expected that its effect on the w.a. stress production will be small. For these field conditions: wave Reynolds number $R_w \approx 1131 \times 10^4$, $k\beta^{-1} \approx 0.00042$ and $(c/u_*)_{cr} \approx 69$ (< 81). On the other hand, since Z (≈ 1.54) is not very large, ky_n^* (≈ 0.00056) and $k\delta_n$ (≈ 0.00037) are larger than $k\delta_*$ (≈ 0.00007), and $\delta_*\beta^{-1}$ (≈ 0.17) is small, we may conclude that the effects of mean wind shear and turbulence on the Stokes layer will be significant. Such effects widen the zone of influence, ky_0^*, and enhance the production of the w.a. stresses by reducing their decay rate D. It is important to note that at sea, u_* is difficult to measure (typical uncertainties are of $O(\pm 15\%)$) and may also depend on the state of wave development which, perhaps, is a function of fetch. Consequently, c/u_* values in the laboratory and in the open ocean may not have one-to-one

† There is some evidence (Morduckhovich & Tsvang 1966; Papadimitrakis *et al.* 1987) that R increases with instability, although such dependence is controversial.

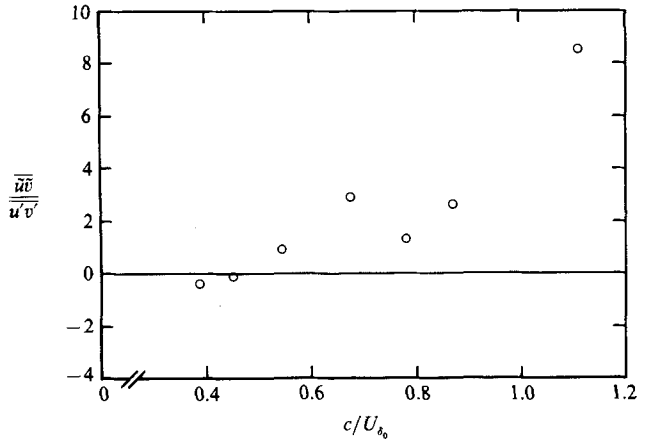

FIGURE 4. Distribution of $\tilde{u}\tilde{v}/\overline{u'v'}$ as a function of dimensionless wave speed.

correspondence. Because this particular experiment was also conducted under unsteady conditions, it will not be further discussed.

Inspection of figure 2 reveals that, at the lowest point of measurements, while the coefficient R' remains constant with dimensionless wave speed, the correlation coefficient R decreases progressively from about 0.3, at $c/U_{\delta_0} \approx 1.11$, to 0.1 at $c/U_{\delta_0} \approx 0.39$ (except at $c/U_{\delta_0} \approx 0.68$). Again, this decrease is caused by a modification of the structure of the airflow field associated with the presence of large-scale (w.c.) velocity perturbations, as can be seen from (3.15). Close to the water surface, $-\tilde{u}\tilde{v}$ decreases toward zero with decreasing dimensionless wave speed (figure 4), owing to the rapid decrease of $\tilde{v}$ perturbations. For $c/U_{\delta_0} \leqslant 0.45$, the w.a. stress remains negative, although small and, therefore, $|\overline{uv}| < |\overline{u'v'}|$. In contrast, $\overline{u'^2}$, $-\overline{u'v'}$ and $\overline{v'^2}$ increase monotonically with decreasing c/U_{δ_0} and, thus, the coefficient R decreases. Since the fractional contributions $\overline{uv}_i/\overline{uv}$ increase with decreasing R (equations (3.17) and (3.18)) and, at the lowest point of measurements, R decreases with decreasing c/U_{δ_0}, it becomes evident that the w.c. perturbations affect the distribution of these contributions under different wind conditions, mainly through variations of their dynamical behaviour and their mutual interaction with turbulence, processes also reflecting the critical- and Stokes-layer dynamics. Variations in surface roughness condition† with wind speed (between the aerodynamically smooth and transitionally rough regimes) may also affect the skewness and diffusion factors $S_{u,v}, D_{u,v}$, as Nakagawa & Nesu (1977) have shown for smooth- and rough-bed open-channel flows, and alter to a small extent the probability density distribution of uv, and ultimately the contributions $\overline{uv}_i/\overline{uv}$.

Figure 5 shows the distribution of the fractional contributions $\overline{\tilde{u}\tilde{v}}_i/\overline{\tilde{u}\tilde{v}}$ $(i = 1, \ldots, 4)$ to the mean w.a. Reynolds stress, at the lowest point of measurements. For $c/U_{\delta_0} \geqslant 0.68$, the entire w.a. stress is produced during the ejection and sweep phases, their contributions being 51% and 49%, respectively. For $c/U_{\delta_0} < 0.68$, a different behaviour is observed. At $c/U_{\delta_0} = 0.55$, the inward and outward contributions are still negligible, but the contributions of ejections and sweeps are different, being 68% and 41%, respectively. At the lowest dimensionless wave speed, the above trend is

† Characterized by the roughness Reynolds number $Re^* = u_* y_0/\nu$ according to traditional measures. The roughness height, y_0 [$= \exp(-\kappa C)$], was calculated from the mean velocity profiles (see I).

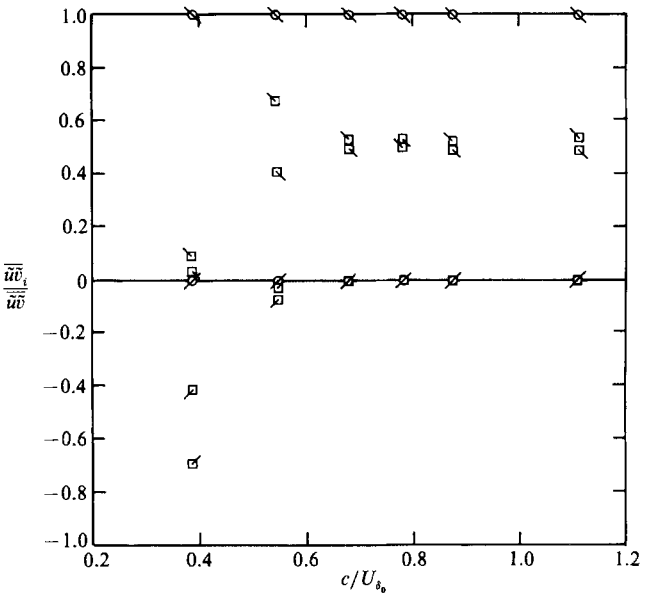

FIGURE 5. Fractional contributions to $\overline{\tilde{u}\tilde{v}}$ and $\overline{u'v'}$ at the lowest point of measurements. ◰, 1st quadrant; ◱, 2nd quadrant; ◲, 3rd quadrant; ◳, 4th quadrant. ⊘, negative contributions; ∅, positive contributions.

reversed, and the $-\overline{\tilde{u}\tilde{v}}$ stress is mainly produced during the wallward and outward interactions, their contributions being −70% and −43%, respectively. Ejections contribute about 8%. This behaviour is expected, since $-\overline{\tilde{u}\tilde{v}} < 0$ at this particular c/U_{δ_0} ratio.

The distribution of the fractional contributions $\overline{\tilde{u}\tilde{v}}_i/\overline{\tilde{u}\tilde{v}}$ with c/U_{δ_0} certainly reflects variations in both the amplitude $(\hat{u}, \hat{v})$ and phase lag $(\theta_{\tilde{u}}, \theta_{\tilde{v}})$ of $\langle\tilde{u}\rangle$ and $\langle\tilde{v}\rangle$ phase averages. In the water proximity, $\theta_{\tilde{v}}$ and $\theta_{\tilde{u}}$ are determined from a kinematic boundary condition and the combined influence of critical and turbulent Stokes layer, respectively. For high and moderate dimensionless wave speeds ($1.10 \leqslant c/U_{\delta_0} \leqslant 0.68$) $\theta_{\tilde{v}}$ approaches 270°, whereas $\theta_{\tilde{u}}$ varies between 135°–90°. At the lower dimensionless wave speeds ($c/U_{\delta_0} < 0.68$), $\theta_{\tilde{v}}$ and $\theta_{\tilde{u}}$ approach 0° and a small positive angle in the first quadrant (i.e. < 90°), respectively, for then the wave behaves as a solid (wavy) boundary and the compression of the flow field below the critical layer is strong. The latter effect also results in a strong reduction of the amplitude of $\hat{v}$, as $\hat{v}$ is related to the undulation of the mean streamlines observed in the frame $x_c^* = x^* - ct^*$ travelling at the wave celerity c. Presumably at low dimensionless wave speeds the shear flow instability, with which the cat's eye is related, induces increased wind-to-wave momentum transfer which, in turn, induces tighter wind-wave coupling and stronger turbulence–mean flow interactions. As a consequence of these variations in $\theta_{\tilde{u}}$ and $\theta_{\tilde{v}}$ with c/U_{δ_0}, the smallest negative peak of $\langle\tilde{u}\rangle$ and the largest positive peak of $\langle\tilde{v}\rangle$ distributions shift downward along the leeward side of the mechanically generated wave crest, as c/U_{δ_0} decreases from 1.11 to 0.39 (see also §4). Then the almost-out-of phase (i.e. 180°) oscillations of $\langle\tilde{u}\rangle$ and $\langle\tilde{v}\rangle$ phase averages, when $c/U_{\delta_0} \geqslant 0.68$, result in negligible $\overline{\tilde{u}\tilde{v}}_1$ and $\overline{\tilde{u}\tilde{v}}_3$ contributions. Conversely, for low dimensionless wave speeds, $0° < \theta_{\tilde{u}} - \theta_{\tilde{v}} \ll 90°$ and $\langle\tilde{u}\rangle$, $\langle\tilde{v}\rangle$ oscillate almost in phase, producing negligible $\overline{\tilde{u}\tilde{v}}_2$ and $\overline{\tilde{u}\tilde{v}}_4$ contributions.

At the lowest point of measurements, independent of dimensionless wave speed,

the fractional contributions $\overline{u'v'_j}/\overline{u'v'}$ ($j = 1, 2$) to the mean turbulent Reynolds stress remain nearly constant, in accord with smooth-wall boundary-layer results; $\overline{u'v'_2}$ is virtually zero so that $\overline{u'v'}$ is entirely produced by $\overline{u'v'_1}$, as figure 5 also shows. This contribution of $\overline{u'v'_1}/\overline{u'v'}$ ($\approx 100\%$) is smaller than the value of 132% (77+52) reported by Kim *et al.* (1971) and Lu & Willmarth (1973) for smooth, flat-wall boundary layers. However, this result is consistent with the observation that both the turbulent Reynolds stress and turbulence intensities are reduced in the presence of mechanically generated waves, as further evidenced by the relatively low roughness length for the wave height.

The results of $\langle \tilde{u}\tilde{v} \rangle$ and $\langle u'v' \rangle$ stress classification suggest that the pronounced rise of $\overline{uv}_i/\overline{uv}$, observed when $c/U_{\delta_0} < 0.68$, can be at least partly attributed to the w.a. stresses. Their reduced contributions (relative to the lower wind speed) counterbalance this rise, and result in constant fractional contributions to the mean turbulent Reynolds stress at all dimensionless wave speeds. Comparing our fractional contributions with those obtained by Takeuchi *et al.* (1975), using McIntosh, Street & Hsu's (1975) data† over wind-generated waves alone where the air flow perturbation by the waves is considered to be small, we conclude that the magnitude of the burst and sweep events is enhanced by the presence of mechanically generated waves.

3.5. *Relative intensities of the various events*

In order to describe clearly the influence of water waves on the bursting process, it is necessary to investigate the relative intensity of each event of the bursting cycle throughout the boundary layer. Figures 6 and 7 show two typical distributions of the fractional contributions of the various events to $\overline{uv}$, $\overline{u'v'}$ and $\overline{\tilde{u}\tilde{v}}$ Reynolds stresses, as a function of either y^*/δ_0 or ky^*. As seen from figure 6, the intensities of the various events satisfy the relation: ejection > sweep > outward interaction > inward interaction, within the observed range of y^*/δ_0 (or ky^*). The difference between outward and inward interactions, however, is very small. This behaviour was also observed by Lu & Willmarth (1973), Nakagawa & Nesu (1977, 1981), and others. Close to the water surface ($0 < y^*/\delta_0 \leqslant 0.14k\delta$ or $0 < ky^* \leqslant 0.3k\delta$), the detailed distribution of the various events depends on the ratio c/U_{δ_0}. The intensity of all events increases with increasing y^*/δ_0 (or ky^*), reaches a maximum, and then either decreases down to a minimum or remains fairly constant. The width and location of the two extrema depend on c/U_{δ_0}. At the lowest dimensionless wave speed, the intensity decreases with increasing y^*/δ_0 (or ky^*), in accord with the results of Lu & Willmarth (1973), Brodkey *et al.* (1974), and Takeuchi *et al.* (1977). Nakagawa & Nesu (1977) observed a similar behaviour for their smooth-bed, open-channel flows, but they found an increase in the intensity of ejections and sweeps with height in their rough-bed case. However, their rough-bed measurements do not extend deeply enough in the wall region (down to about $y^*/\delta \approx 0.085$) and, thus, it is unknown whether these trends continue there.

In the equilibrium region ($0.14k\delta < y^*/\delta_0 \leqslant 0.28k\delta$ or $0.3k\delta < ky^* \leqslant 0.6k\delta$) the intensity of each event is nearly constant, independent of position, (which is a further proof that, in this region, the bursting process and the accompanying turbulence production attain a stable equilibrium state). On the other hand in the free stream ($y^*/\delta_0 > 0.28k\delta$ or $ky^* > 0.6k\delta$) it increases rapidly with y^*/δ_0, as reported by all previously mentioned investigators.

Again, the differences among these distributions ($\overline{uv}_i/\overline{uv}$) in the water proximity

† These data show much lower contributions from each quadrant than their mechanically generated wave counterparts and are consistent with Lu & Willmarth's (1973) estimates.

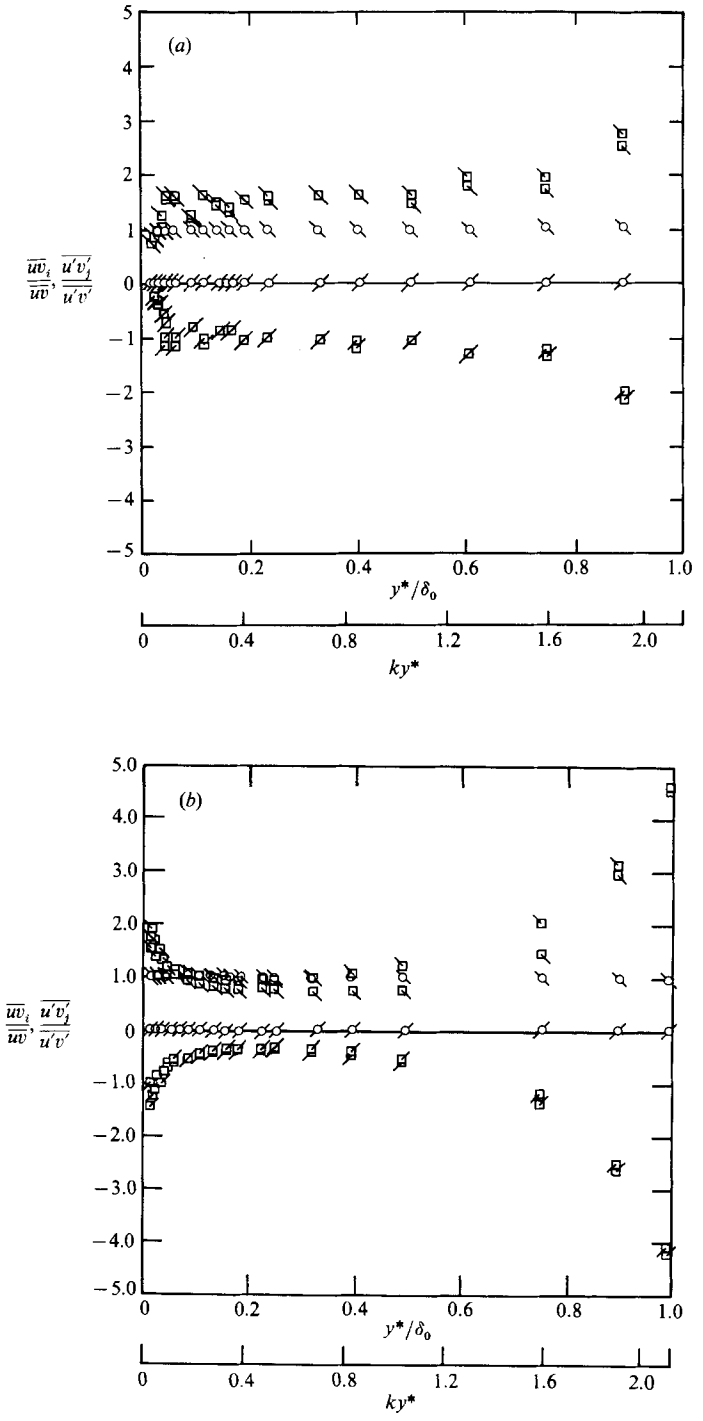

FIGURE 6. Distributions of $\overline{uv}_i/\overline{uv}$ and $\overline{u'v'_i}/\overline{u'v'}$ throughout the boundary layer, at $H = 0$. Notation as in figure 5. (*a*) $c/U_{\delta_0} = 1.11$; (*b*) $c/U_{\delta_0} = 0.39$.

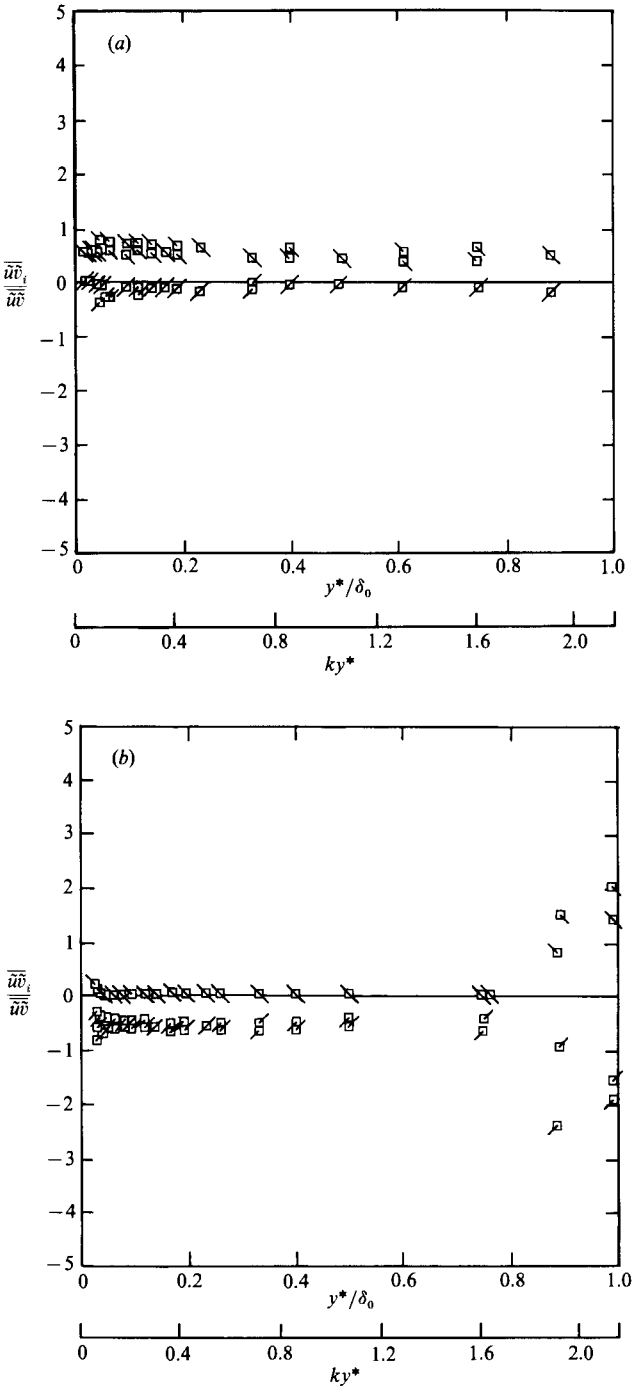

FIGURE 7. Distributions of $\overline{\tilde{u}\tilde{v}}_i/\overline{\tilde{u}\tilde{v}}$ throughout the boundary layer, at $H = 0$. Notation as in figure 3. (*a*) $c/U_{\delta_0} = 1.11$; (*b*) $c/U_{\delta_0} = 0.39$.

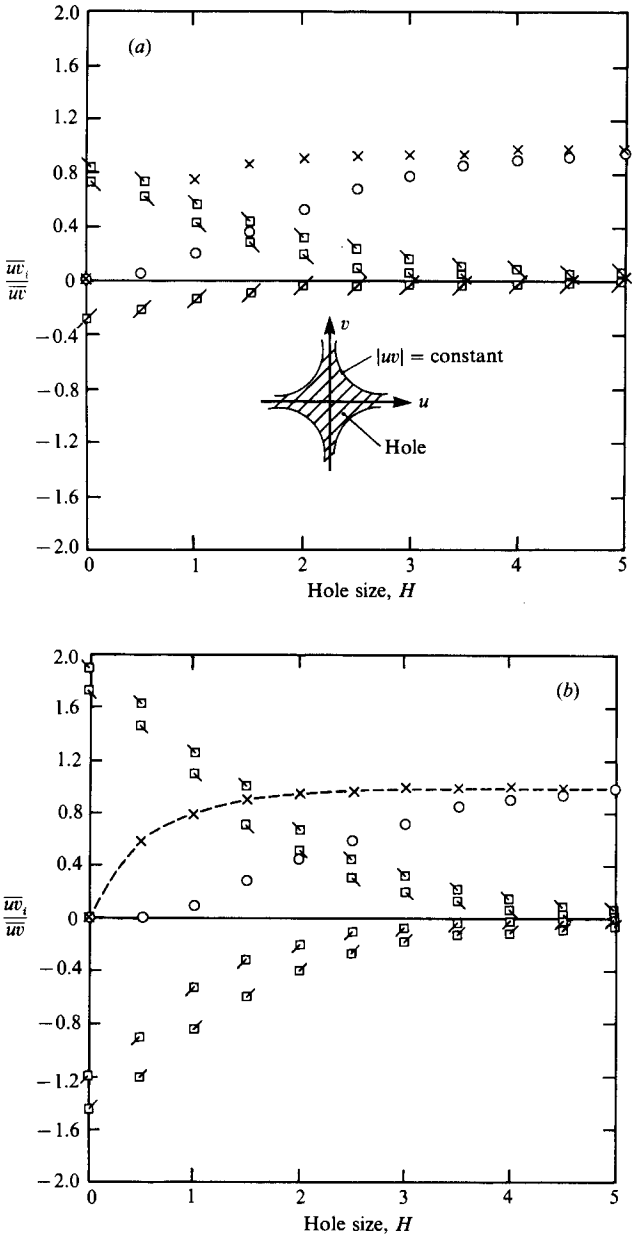

FIGURE 8. Measurements of the contributions to $\overline{uv}$ from different events. ◰, 1st quadrant; ◱, 2nd quadrant; ◲, 3rd quadrant; ◳, 4th quadrant; ○, hole; ×, fraction of time spent in the hole. (*a*) $c/U_{\delta_0} = 1.11$; (*b*) $c/U_{\delta_0} = 0.39$.

(i.e. for $ky^* < 0.3k\delta$) can be attributed to variations of the dynamical behaviour of the w.a. Reynolds stress and the increasing modulation of wind turbulence by the waves with decreasing dimensionless wave speed. It is in this region that virtually all of the w.a. stresses are produced (see Hsu & Hsu 1983; and I). For $ky^* \geqslant 0.3k\delta$, $|\tilde{u}\tilde{v}|$ and the oscillatory part of both $\tilde{u}\tilde{v}$ and $u'v'$ become negligible at all dimensionless wave speeds, and the influence of waves on the fractional contribution $\overline{uv}_i/\overline{uv}$ becomes insignificant.

As seen from figure 7, the distribution of fractional contributions

$$\overline{u'v'_j}/\overline{u'v'} \ (j = 1, 2)$$

to the mean turbulent stress $-\overline{u'v'}$ remains invariable throughout the boundary layer, whereas the distribution of $\overline{\tilde{u}\tilde{v}_i}/\overline{\tilde{u}\tilde{v}}$ $(i = 1, \ldots, 4)$ shows trends similar to those of $\overline{uv_i}/\overline{uv}$ but somewhat more erratic. The oscillatory behaviour of the $-\overline{\tilde{u}\tilde{v}}$ stresses with height and their small magnitude in the free stream are certainly responsible for such erratic distributions. The influence of these oscillations, which were shown to be a consequence of the turbulence-modified Stokes layer, and the contribution of the w.a. stresses produced by the critical layer are clearly reflected on the distributions $\overline{\tilde{u}\tilde{v}_i}/\overline{\tilde{u}\tilde{v}}$ in the water proximity. The almost constant relative intensity equilibrium range, and the sharp rise of these intensities in the free stream are also shown in figure 7.

Since both the time- and phase-averaged $\tilde{u}\tilde{v}$ and $u'v'$ stress distributions depend on the critical- and Stokes-layer behaviour (which, in turn, is affected by turbulence diffusion and mixing), it becomes apparent once more that these layers influence the Reynolds stress generation processes in the boundary layer above mechanically generated water waves.

3.6. *Reynolds stress classification*

Figure 8 shows typical contributions to the mean Reynolds stress $\overline{uv}$ of the various events of the bursting cycle, at the lowest point of measurements, as a function of the 'hole' size H. The fraction of time spent in the 'hole' region is also included in these figures. As seen from the contribution curve related to the 'hole', for a large portion of the time $|uv|$ is very small. Ejections are always the largest contributor to $\overline{uv}$, with sweeps the second largest, independent of dimensionless wave speed and 'hole' size. The contributions from $\overline{uv}_1$ and $\overline{uv}_3$ are relatively small, except for $c/U_{\delta_0} < 0.68$. Thus, the importance of the ejection-like events in the turbulent boundary layer over progressive water waves is obvious.

The time occupied by the 'hole' is very large and, hence, we can infer that ejections may arise in the form of sharp pulses. The fractions of time $T_i(H)$ spent by the uv signal in the ith quadrant have also been calculated as a function of H. The fractions of time $T_{1,3}$ spent in the first and third quadrants (not shown in figure 8) were found to be approximately equal, with T_1 slightly greater than T_3 at low dimensionless wave speeds. T_4 was found to be somewhat greater than T_2, with a tendency to become equal at low c/U_{δ_0} values. The fact that $T_2 \approx T_4$ shows that sweeps are probably as energetic as ejections. These results agree well with the observations of Corino & Brodkey (1969), Kim *et al.* (1971), Grass (1971), Lu & Willmarth (1973), Brodkey *et al.* (1974), and Nakagawa & Nesu (1977). Table 4 lists the values of $T_{2,4}$ at $H = 0$.

Following Lu & Willmarth (1972) and Nakagawa & Nesu (1977), we have also derived expressions for $T_{2,4}(0)$ as a function of R, $S_{u,v}$ and $D_{u,v}$, namely

$$T_{2,4}(0) = \frac{\cos^{-1}(-R)}{2\pi} \pm \frac{S^-}{6(2\pi)^{\frac{1}{2}}}, \qquad (3.19a, b)$$

and similar expressions hold for $T_{1,3}(0)$. The corresponding expressions for any threshold H are too complicated and will not be given here. As seen from table 4, the values $T_{2,4p}(0)$ (where the subscript p indicates 'predicted') calculated from (3.19*a*, *b*) with S^- being neglected since its contribution to $T_{2,4}(0)$ is $\leqslant 4\%$, and our experimental results both decrease as R decreases from 0.29 to 0.1. The former are also remarkably close to their experimental counterparts. Again, the contribution of

U_{δ_0} (cm/s)	141	179	200	231	285	346	402
R	0.29	0.26	0.23	0.31	0.18	0.13	0.10
$T_2\ (H=0)$	0.293	0.287	0.284	0.295	0.274	0.265	0.260
$T_4\ (H=0)$	0.306	0.302	0.293	0.309	0.286	0.274	0.270
$T_{2,4\mathrm{p}}\ (H=0)$	0.297	0.292	0.287	0.300	0.279	0.271	0.266

TABLE 4. Dimensional ejection and sweep time periods

S^- to $T_{2,4}(H=0)$ causes $T_{2\mathrm{p}}(H=0)$ to slightly decrease and $T_{4\mathrm{p}}(H=0)$ to increase, relative to their values with $S^-=0$, bringing them even closer to their experimental values.

In contrast to our results, Kawamura & Toba's (1985) observations over wind-generated waves (for which $c/u_*=1.15, c/U_{\delta_0}=0.064$) have shown that $T_2\approx 1.3T_4$. However, as we demonstrate below, our results are not inconsistent with their finding. In this respect, it is interesting to note that Nakagawa & Nesu (1977) have shown that the ratio $T_4(0)/T_2(0)$: (i) decreases from about 1.3 to 0.8 as S^- decreases from $+0.6$ to -0.4; (ii) remains <1.0 for $S^->0$; and (iii) becomes >1.0 for $S^-<0$. At $S^-=0$ their calculations indicate that $T_4/T_2=1.0$. They have also shown that for rough surfaces S^- becomes negative, at least close to the open-channel bed. It is then possible that, for wind-generated waves at sufficiently low dimensionless wave speeds where the water surface becomes hydrodynamically rough (and air flow separation usually occurs), S^- may become negative. This conclusion is indeed supported by the turbulence measurements of Buckles, Hanratty & Adrian (1984) in the air above *steep* solid wavy surfaces. They found that in such flows separation and reattachment occur, and the skewness of horizontal velocity fluctuations, S_u, changes sign at about the height of maximum turbulent intensity, being positive close to the wall. However, in smooth flows above small-steepness (unseparated) mechanically generated water waves $S^u<0$. Since in general $|S_u|>|S_v|$, it can be argued that for $S_u>0$, S^- will be negative. Therefore, Kawamura & Toba's (1985) finding that $T_2>T_4$ does not necessarily contradict our results which indicate otherwise.

The distributions of the normalized contribution of ejection and sweep events throughout the boundary layer, at $H=0$, namely

$$-\frac{\overline{uv}_2}{\{(\overline{u^2})\,(\overline{v^2})\}^{\frac{1}{2}}};\qquad -\frac{\overline{uv}_4}{\{(\overline{u^2})\,(\overline{v^2})\}^{\frac{1}{2}}}$$

shown in figure 9, are nearly independent of dimensionless height, except close to the water surface and at the edge of the boundary layer. Figure 10 shows the distribution of these contributions, at the lowest point of measurements, as a function of dimensionless wave speed. For $c/U_{\delta_0}=0.39$, it was found that

$$-\frac{\overline{uv}_2}{\{(\overline{u^2})\,(\overline{v^2})\}^{\frac{1}{2}}}\approx 0.26;\qquad -\frac{\overline{uv}_4}{\{(\overline{u^2})\,(\overline{v^2})\}^{\frac{1}{2}}}\approx 0.20,$$

but similar values are expected for the higher dimensionless wave speeds, judging from their distribution at the lowest point of measurements. Lu & Willmarth (1973) reported values of 0.34 and 0.24, respectively.

The average value of the ratio $\overline{uv}_2/\overline{uv}_4$, at the lowest point of measurements, is approximately 1.15, being smaller than either of the values 1.45 and 1.85 reported, respectively, by Kawamura & Toba (1985) and Lu & Willmarth (1973). For $c/U_{\delta_0}>$

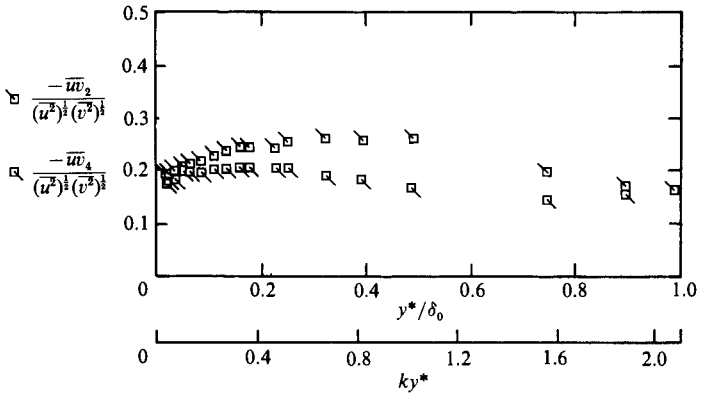

FIGURE 9. Typical distributions of normalized ejections and sweep contributions. ⊠, ejections; ⊡, sweeps. $c/U_{\delta_0} = 0.39$.

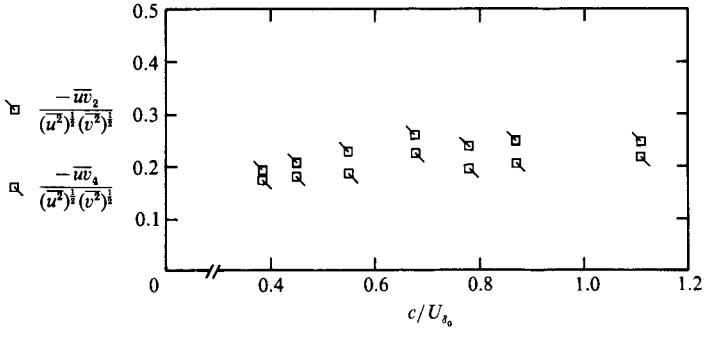

FIGURE 10. Distribution of normalized ejection and sweep contributions, at the lowest point of measurements, as a function of dimensionless wave speed. Notation as in figure 9.

0.68, this ratio decreases near the interface (indicating that sweeps become even more energetic compared with moderate and low dimensionless wave speeds), but remains nearly constant in the inner and equilibrium regions of the boundary layer with values between 0.95–1.15, as opposed to 1.35 reported by Lu & Willmarth (1973). As c/U_{δ_0} decreases, $\overline{uv}_1/\overline{uv}_4$ increases towards a value of approximately 1.4 in the equilibrium and most of the free-stream regions, with a tendency to decrease in the centreline region of the channel. This trend of increasing $\overline{uv}_2/\overline{uv}_4$ towards the equilibrium region at low dimensionless wave speeds agrees well with the observations of Wallace *et al.* (1972), Brodkey *et al.* (1974), and Nakawaga & Nesu (1977). From these characteristics, as well as from the contributions to $\overline{uv}$ of the various events, it appears that the bursting process near the free-stream may consist of smoother and more isotropic events, independent of flow type and surface roughness condition. Such universal behaviour may be attributed to the effects of pressure fluctuations in forcing the turbulent field towards isotropy (Elliott 1972).

3.7. *Ejection and sweep time periods*

An estimate of the characteristic mean time periods related to ejections and sweeps was obtained from the Reynolds stress classification according to the hole method. Figure 11 shows the distribution of the non-dimensional mean time interval $\overline{T}_{e,s} = T_{e,s} U_{\delta_0}/\delta_1$ between ejections and/or sweeps, at the lowest point of measurements, as a function of H and c/U_{δ_0} as a parameter; δ_1 denotes the displacement thickness

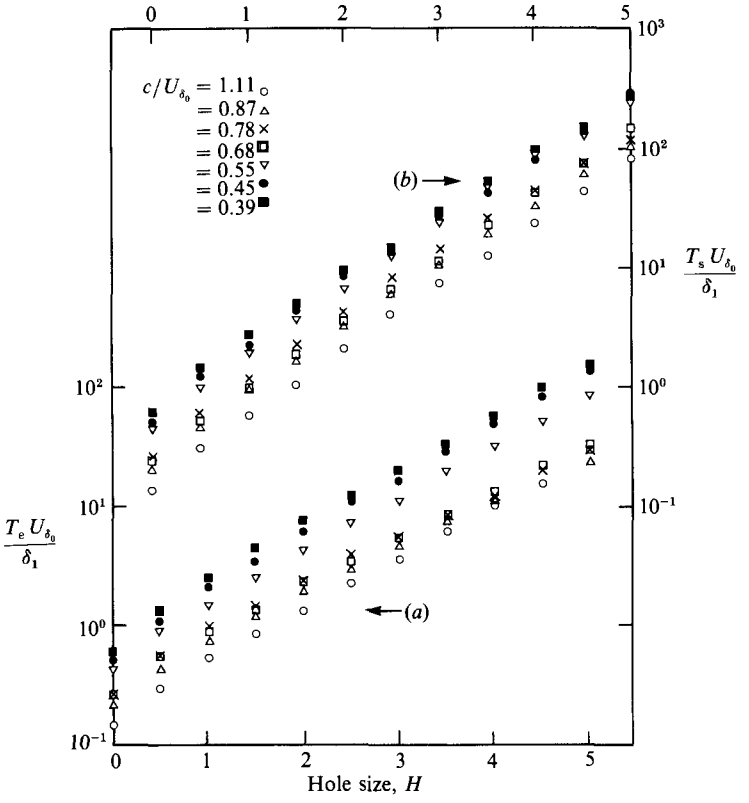

FIGURE 11. Distributions of non-dimensional mean time interval between: (*a*) ejections and (*b*) sweeps, at the lowest point of measurements, as a function of hole size H. Left and right arrows point to the respective coordinate.

calculated from the mean velocity data. It is seen that these time intervals have a remarkably log–linear behaviour, but they do not scale with the outer flow variables U_{δ_0} and δ_0, as suggested by Rao, Narasimha & Badri-Narayanan (1971) and by Lu & Willmarth (1973). They also increase with both the wind speed and the hole size H, except at $c/U_{\delta_0} = 0.68$. The corresponding distributions of the number of ejection and sweep occurrences $N_{e,s}$, shown in figure 12, are remarkably less scattered, providing further evidence for the lack of scaling of the bursting periods with the outer flow variables. $N_{e,s}$ are related to $T_{e,s}$ through the following relationship:

$$T_{2,4}(H) = \frac{0.002\,N_{e,s}}{184.32} = \frac{0.002}{T_{e,s}}. \qquad (3.20a, b)$$

The coefficients 0.002 and 184.32 correspond to the sampling time interval and record length in seconds, respectively. Figure 13 shows the distribution of $\bar{T}_{e,s}$ at $c/U_{\delta_0} = 0.39$, as a function of the hole size H and y^*/δ_0 as a parameter. The results clearly suggest that the mean non-dimensional time intervals: (i) have similar distributions; and (ii) are height dependent (except for $H = 0$, where $\bar{T}_e$ and $\bar{T}_s$ are nearly equal and independent of y^*/δ_0 and c/U_{δ_0}). This behaviour was also observed by Lu & Willmarth (1973), Brodkey *et al.* (1974), and Nakagawa & Nesu (1977) for both the smooth and rough flow regimes. The data also indicate that N_e (or T_e) increase (or decrease) up to about $y^*/\delta_0 \approx 0.39$ (or $ky^* \approx 0.85$). At higher elevations this trend is reversed. Bogard & Tiederman (1986) found that the number of ejections

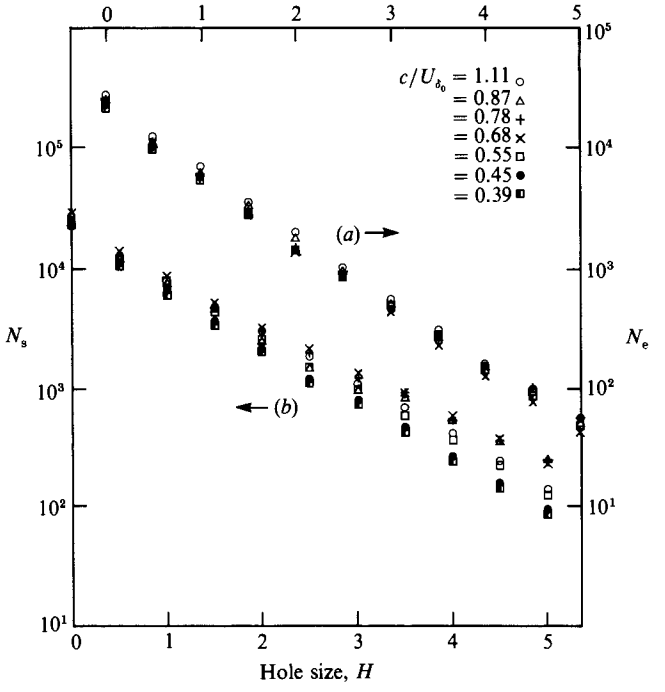

FIGURE 12. Distributions of the number of: (*a*) ejection and (*b*) sweep occurrences, at the lowest point of measurements, as a function of hole size H.

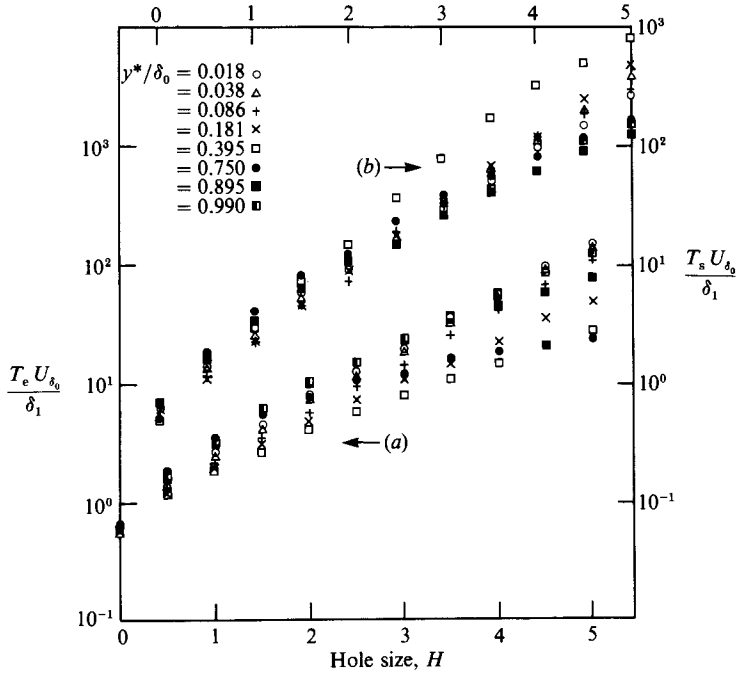

FIGURE 13. Typical distributions of non-dimensional mean time interval between: (*a*) ejections and (*b*) sweeps throughout the boundary layer, as a function of hole size H. $c/U_{\delta_0} = 0.39$

in a burst increased substantially away from the wall, up to about $y^+ \approx 100$, and then slowly decreased from that point towards the centreline of the channel. They attributed this increase to the breakup of the streak filament (which formed one ejection near the wall) into multiple ejections far from the wall. However, their data indicated that despite this increase the number of bursts remained constant throughout the boundary layer.

The absence of a plateau in the variation of $\bar{T}_{e,s}$ with H (figure 13) indicates that the value of H alone is not an acceptable criterion for determining the actual values of the non-dimensional mean ejection and sweep rates. The unique features observed by Lu & Willmarth (1973) that: (i) 'when H reaches a value between 4 and 4.5 only $\overline{uv}_2/\overline{uv}$ is not zero, regardless of the distance from the wall'; and (ii) 'at $H = 2.25$ to 2.75, the contributions from $\overline{uv}_1$, $\overline{uv}_2$ and $\overline{uv}_3$ vanish at any distance from the wall,' were not found in this study. Nor could these features be observed at any other value of H. Above $H = 5$, the contributions of all events become negligible. Blackwelder & Haritonidis (1983) also found that no unique value of their threshold could be obtained with the VITA method by searching for a region where the bursting frequency was relatively independent of the threshold. These observations, however, are consistent with the findings of Chen & Blackwelder (1978) who showed that, whenever a simple threshold level (such as H) is applied to a function having a continuous probability distribution (such as uv), the frequency of occurrence of the detected event will vary monotonically with the threshold parameter. Therefore, with the 'hole' and other detection methods, almost any value of $\bar{T}_{e,s}$ can be obtained by choosing particular values of the threshold H. Consequently, no great significance can be placed on the absolute values of $\bar{T}_{e,s}$ recorded. However, if H is held constant for all of the data, the relative variation of the estimated period cannot be attributed to the threshold value (see also §4).

For $H \approx 3$–4, $\overline{uv}_1/\overline{uv}$ and $\overline{uv}_3/\overline{uv}$ become very small, but ejections still contribute up to 15–40% to the mean Reynolds stress throughout the boundary layer, whereas $\overline{uv}_4/\overline{uv}_2 \approx 0.45$. Since $|uv| = H(\overline{u^2})^{\frac{1}{2}}(\overline{v^2})^{\frac{1}{2}}$ and $R = -\overline{uv}/(\overline{u^2})^{\frac{1}{2}}(\overline{v^2})^{\frac{1}{2}}$, it follows that $|uv| = (H/R)|\overline{uv}|$. Close to the water surface, for high and moderate c/U_{δ_0} values, $R \approx 0.3$ and, therefore, $H/R \approx 10$. For the lower dimensionless wave speeds, H/R will be even greater owing to the reduced values of R. Ejections that correspond to such threshold levels are certainly violent and must come from large spikes in the uv signal. As seen from figure 11, the non-dimensional mean ejection and sweep time periods do not remain constant but increase with increasing Reynolds number for any H = constant (including $H = 4$), in accord with the conclusions of Bogard & Tiederman (1983). The non-dimensional mean time intervals $\bar{T}_{e,s} = T_{e,s}\, u_*^2/\nu$, scaled with the inner variables and corresponding to $H = 4$, also increase with (the conventionally defined) momentum-thickness Reynolds number, Re_θ, as shown in table 5. The same holds true for any other value of the threshold and/or location y^*/δ_0 throughout the boundary layer. Nor could any of these time intervals be scaled with the geometrical mean of the inner and outer timescales, as suggested by Alfredsson & Johansson (1982) for solid-wall flows. Since the viscous length of the hot films we used was < 20, we have no reason to believe that our results are contaminated by wire-length effects, as discussed by Blackwelder & Haritonidis (1983) and Alfredsson & Johansson (1983). Jackson (1976) has also pointed out that none of the data from boundary-layer flows in rivers with smooth and rough beds supports this scaling, at least with the outer flow parameters.

Table 5 also shows the dimensional ejection time intervals T_e which correspond to $H = 4$. They do not appear to increase or decrease monotonically with decreasing

c/U_{δ_0}	1.11	0.87	0.78	0.68	0.55	0.45	0.39
Re_θ	4180	4620	5100	6460	6050	7500	9150
$\tilde{T}_e$ $(H = 4)$	51	66	80	109	339	611	1065
$\tilde{T}_s$ $(H = 4)$	125	201	286	354	928	1053	1814
T_e $(H = 4)$	0.443	0.341	0.326	0.325	0.511	0.673	0.685
T_e $(H/R = 10)$	0.149	0.100	0.080	0.145	0.057	0.038	0.032
$\overline{uv}_2/\overline{uv}$ $(H/R = 10)$	0.18	0.20	0.42	0.18	0.53	0.87	0.25
$\overline{uv}_4/\overline{uv}$ $(H/R = 10)$	0.09	0.12	0.12	0.08	0.34	0.68	1.07
$\max\langle uv_2\rangle/\overline{uv}$	3.15	2.95	2.73	2.53	2.82	3.08	3.32

TABLE 5. Non-dimensional ejection and sweep time periods

dimensionless wave speed. Such a trend, however, is not totally inconsistent with the findings of Bogard & Tiederman (1983, 1986) which suggest that the number of ejections within a single burst may vary under different Reynolds-number conditions, thereby causing variations in T_e. Quantitatively, the lack of monotonicity in the variation of $T_e(H = 4)$ with decreasing dimensionless wave speed may be explained by the fact that the number of ejections detected, whenever $|uv| > (H/R)|\overline{uv}|$ at $H = 4$, is affected by variations in the stress threshold H/R caused by variations in R. Therefore, the values of T_e that correspond to the fixed threshold $H/R = 10$ for all dimensionless wave speeds may be more representative of the time interval between ejections that belong to the same burst. These dimensional time intervals are also shown in table 5. It is interesting to note that these ejection periods correspond closely to the time between the two largest consecutive peaks of the phase-averaged (total) Reynolds stress distributions. The latter can be described by the following approximate equation:

$$\langle uv\rangle \approx \langle\tilde{u}\tilde{v}\rangle + \langle u'v'\rangle = \tfrac{1}{2}|\tilde{u}|\,|\tilde{v}|\cos(2\omega t - \theta_{\tilde{u}} - \theta_{\tilde{v}}) + |\tilde{r}_{12}|\cos(\omega t - \theta_{\tilde{r}_{12}}) + \tfrac{1}{2}|\tilde{u}|\,|\tilde{v}|\cos(\theta_{\tilde{u}} - \theta_{\tilde{v}}) + \overline{u'v'}. \quad (3.21)$$

Here $|\,|$ denotes amplitude and $\tilde{r}_{12} = \langle u'v'\rangle - \overline{u'v'}$ is the w.c. turbulent stress. The existence of multiple peaks in the $\langle uv\rangle$ distributions is consistent with the presence of multiple peaks in both experimentally observed and predicted phase-averaged distributions of the w.c. pressures over mechanically and/or wind-generated waves (Papadimitrakis *et al.* 1986; Okuda 1983; Chalikov 1986), provided that an oscillating shear stress is roughly equivalent to an oscillatory pressure (Longuet-Higgins 1969). It can also be justified by the presence of the w.a. and w.c. Reynolds stresses and their harmonics, as shown in (3.21). The main component of the $\langle\tilde{u}\tilde{v}\rangle$ w.a. stress appears at 2 Hz, with a time interval between successive negative or positive peaks of about 0.5 s. This stress, then, interacts with its w.c. counterpart (producing two more extrema in the $\langle uv\rangle$ distributions) and modulates the above time interval (≈ 0.5 s) according to the phase lags of $\theta_{\tilde{u}}$, $\theta_{\tilde{v}}$ and $\theta_{\tilde{r}_{12}}$. The presence of four peaks in the $\langle uv\rangle$ distributions described by (3.21) is also apparent from the quartic algebraic equation in ωt obtained by letting $\partial\langle uv\rangle/\partial t = 0$. Furthermore, it can be shown that two of these consecutive peaks correspond to the ejection stage of the bursting cycle, that is to the condition: $\langle u\rangle < 0, \langle v\rangle > 0$, and that the other two correspond to the sweeping stage of the cycle (i.e. $\langle u\rangle > 0; \langle v\rangle < 0$). The calculated ejection time periods from the smoothed $\langle uv\rangle$ distributions given by (3.21) agree well with the values obtained from their experimental counterparts, as can be seen in figure 14. The latter shows typical phase-averaged distributions of $\langle\tilde{\eta}\rangle$, $\langle u\rangle$, $\langle v\rangle$ and $\langle uv\rangle$ at

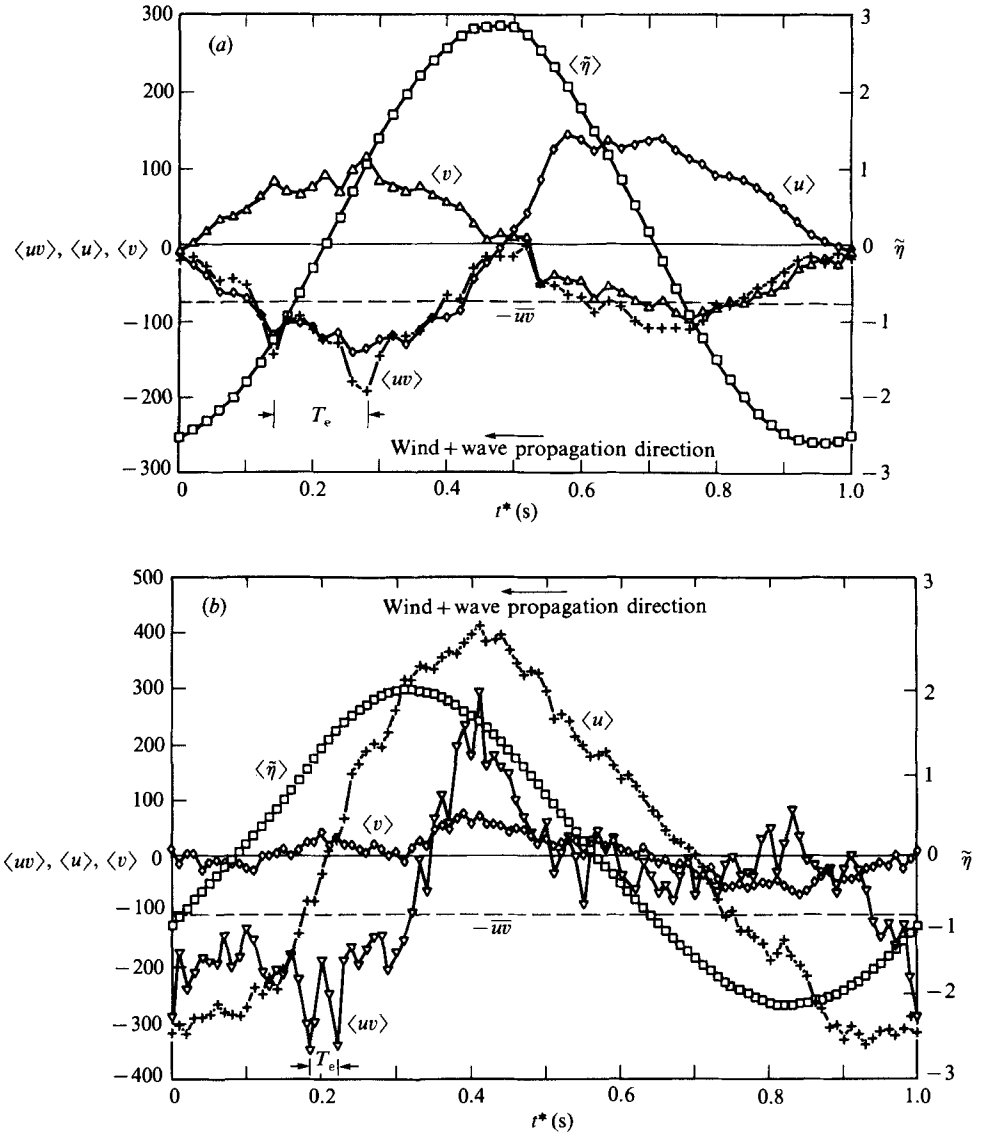

FIGURE 14. Typical phase-averaged distributions of $\tilde{\eta}, u, v$, and of the total Reynolds stress. (*a*) $c/U_{\delta_0} = 0.68$: □, $\langle\tilde{\eta}\rangle$ (cm); ◇, $\langle u\rangle$ (mm/s); △, $\langle v\rangle$ (mm/s); +, $\langle uv\rangle$ (cm^2/s^2). (*b*) $c/U_{\delta_0} = 0.39$: □, $\langle\tilde{\eta}\rangle$ (cm); +, $\langle u\rangle$ (mm/s); ◇, $\langle v\rangle$ (mm/s); ▽, $\langle uv\rangle$ (cm^2/s^2). The horizontal dashed line indicates the value of $-\overline{uv}$, and the vertical arrows point out the two consecutive extreme values of the $\langle uv\rangle$ distribution which correspond to the ejection stage.

two different dimensionless wave speeds. Owing to small contributions from higher (w.c. velocity) harmonics, the measured $\langle uv\rangle$ distributions show a number of minor peaks, but also indicate the presence of four major peaks contributed by the w.a. and w.c. turbulent stresses (perhaps less clearly at low c/U_{δ_0} values). It is also seen in figure 14 that the peak value of the phase-averaged $\langle uv\rangle$ stress distributions which corresponds to the ejection stage of the cycle is about (2.5–3.5) $\overline{uv}$. The ratios max $\langle uv_2\rangle/\overline{uv}$ (for all of the wind speeds examined) are also included in table 5. They decrease with decreasing c/U_{δ_0} only when $c/U_{\delta_0} \geqslant 0.68$. These values are consistent

with the results of bursting detection described by Lu & Willmarth (1973) which indicate that $\max \langle uv_2 \rangle / \overline{uv} \approx 2.6$. Willmarth (1975) has also reported that the ratio $\max \langle uv_2 \rangle / \overline{uv}$ may attain values of up to about 5.5 at times slightly delayed with the respect to the detection of a burst at a nearby location. All of these observations provide further confidence that the Quadrant (Hole) technique at $H/R = 10$ yields reliable ejection time periods for flows above water waves. Therefore, the ejection period in such flows is roughly determined by both the wind speed and the moving-boundary characteristics.

As seen from table 5, $T_e(H/R = 10)$ now decreases with decreasing dimensionless wave speed (with an exception at $c/U_{\delta_0} = 0.68$ where R increases), a behaviour consistent with the fact that as the threshold H ($= 10R$) decreases more ejection events are being detected within the given record length. This observation is also in agreement with: (i) the increased ejection fractional contributions, $\overline{uv}_2/\overline{uv}$, found at high wind speeds; and (ii) the measurements of Lu & Willmarth (1977) and Kawamura & Toba (1985) which indicate that, since the convection velocity of a coherent structure increases with the wind speed (being proportional to U_{δ_0}), more coherent structures are expected to pass through the detecting probe within a wave period as the wind speed increases. At $c/U_{\delta_0} = 1.11$ and 0.68 the respective correlation coefficients R (0.29, 0.31) and ejection time periods $T_e(H/R = 10)$ (0.149, 145 s) are approximately equal. Then, it is interesting to note that the measurements of Kawamura & Toba (1985) at a height $y^*/\delta_0 = 0.133$ over purely wind-generated waves, under a ($U_{\delta_0} =$) 5.75 m/s wind speed for which $R \approx 0.32$, have also yielded $T_e = 0.151$ s. However, no further comparisons will be made because of the limited data available. Again, the $\overline{uv}_{2,4}/\overline{uv}$ fractional contributions at $c/U_{\delta_0} = 0.68$ are very similar to those obtained at $c/U_{\delta_0} = 1.11$, provided that the correlation coefficients R at the corresponding measurement points are approximately equal. Since the value of $c/U_{\delta_0} \approx 0.68$ represents a threshold between the flow regimes of high and low critical layer, and the lowest point of measurements at the various dimensionless wave speeds considered do not correspond to the same dimensional, or more importantly non-dimensional, height (say y^+), it is perhaps not surprising that these fractional contributions are different at c/U_{δ_0}.

For completeness, the ejection and sweep fractional contributions to $\overline{uv}$ which correspond to $H/R = 10$ are also included in table 5. They have a trend similar to that shown in figure 3, but they are smaller than the corresponding values at $H = 0$. It should be noted, however, that the former contributions come only from large ejections.

3.8. *Turbulence production*

The distributions of normalized total, w.a., and turbulent energy productions, $P_n = P\kappa y^*/u_*^3$, $\tilde{P}_n = \tilde{P}\kappa y^*/u_*^3$ and $P'_n = P'\kappa y^*/u_*^3$ throughout the boundary layer are shown in figure 15. Here $P = -\overline{uv}(\partial U/\partial y^*)$, $\tilde{P} = -\tilde{u}\tilde{v}(\partial U/\partial y^*)$, and $P' = -\overline{u'v'}(\partial U/\partial y^*)$. For $y^+ \geqslant 45$, the mean velocity gradient was obtained from (3.1) and was found to agree very well with its value determined from mean velocity data. In the logarithmic region of a typical turbulent boundary layer over a smooth, flat wall, $P_n \approx 1.0$, and values as high as 1.4 have been found in the buffer zone of transitionally rough and fully rough boundary layers (Ligrani & Moffat 1986). For $0.68 \leqslant c/U_{\delta_0} \leqslant 1.11$, most of the w.c. flow in the turbulent boundary layer is below the critical layer; $\tilde{u}, \tilde{v}$ are strongly affected by the Stokes layer and the w.a. stress is the major contributor to the production of the total Reynolds stress. Although the small-scale turbulence production P' is reduced as a result of the large- and small-scale velocity interactions, the total energy production is enhanced owing to the

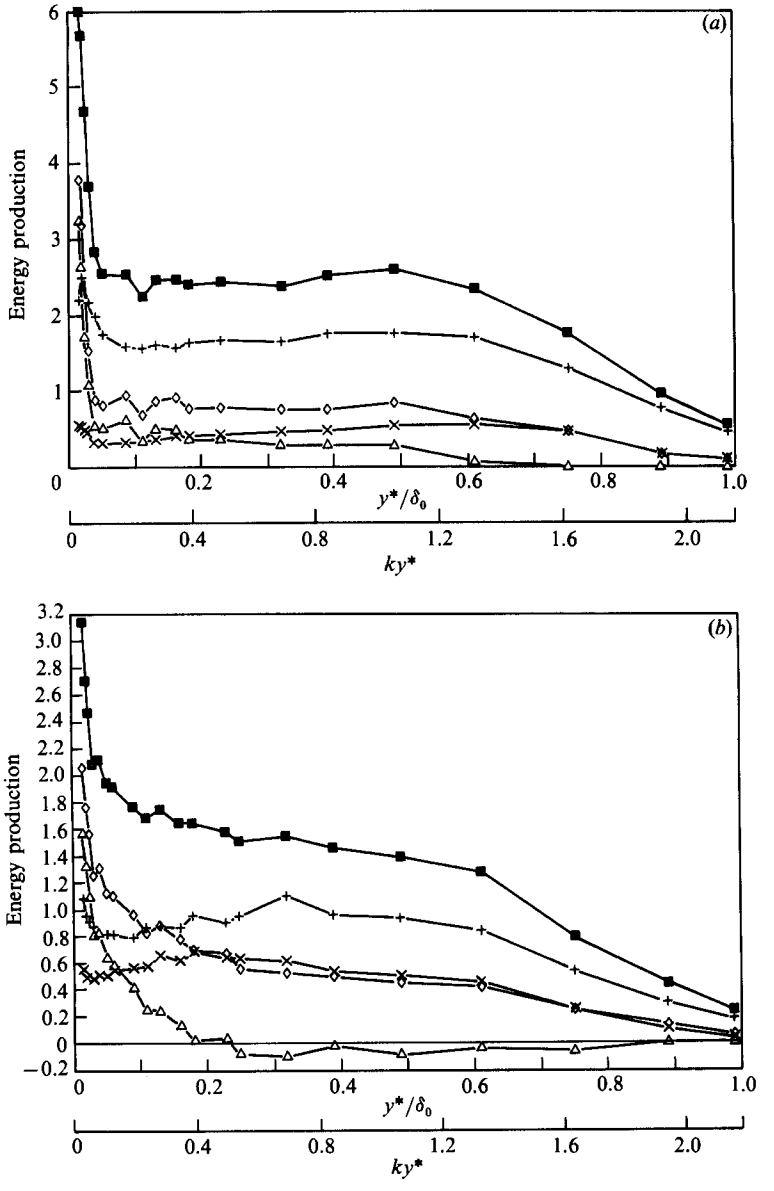

FIGURE 15(*a*,*b*). For caption see facing page.

contribution of the w.a. stress. As seen from figure 15, P_n attains values as high as ≈ 3.8 in the water proximity. When $0.39 \leqslant c/U_{\delta_0} < 0.68$, the w.a. stress contribution to P_n in the same region decreases substantially with decreasing dimensionless wave speed (although P'_n increases with wind speed but remains always < 1.0), thereby causing a reduction in the total energy production P_n. The largest magnitude of inner-region normalized production is found at the highest c/U_{δ_0} value. This is consistent with the results shown in figure 4 which indicate that the ratio $\tilde{u}\tilde{v}/\overline{u'v'}$ becomes maximum there, and the fact that $-\tilde{u}\tilde{v}/U_\infty^2$ becomes also maximum. Figure 15 also shows the distributions of the normalized total energy productions associated with positive ($\tau^+ = -\overline{uv}_2 - \overline{uv}_4$) and negative ($\tau^- = \overline{uv}_1 + \overline{uv}_3$) contributions to $-\overline{uv}$,

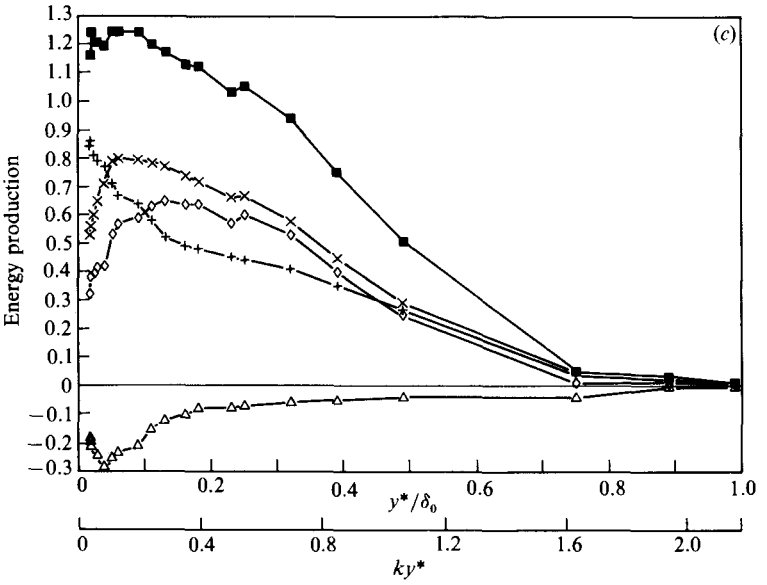

FIGURE 15. Distributions of normalized total (P_n), wave-associated ($\tilde{P}_n$), and turbulent (P'_n) energy productions, as well as of normalized positive (P_n^+) and negative (P_n^-) energy productions. (*a*) $c/U_{\delta_0} = 1.10$; (*b*) $c/U_{\delta_0} = 0.68$; (*c*) $c/U_{\delta_0} = 0.39$. ■, P_n^+; +, P_n^-; ◇, P_n; △, $\tilde{P}_n$; ×, P'_n.

throughout the boundary layer. As seen, the contribution of τ^- to the net production is always smaller than the contribution of τ^+ (but not insignificant), at least up to the equilibrium region. However, in the free stream it becomes of the same order as P_n, though its absolute value is small. Therefore, the energy interchange from turbulence and the w.c. field to the mean flow cannot and should not be neglected.

4. Discussion

The increased contributions of the bursting events to the total mean Reynolds stress and their pronounced rise for $c/U_{\delta_0} < 0.68$, owing to the w.a. stress, strongly suggest that the presence of mechanically generated water waves definitely affects the mechanism of Reynolds stress production near the water surface. The variation throughout the boundary layer of both the distribution of the fractional contributions, $\overline{uv}_i/\overline{uv}$, and of the ratio $\overline{uv}_2/\overline{uv}_4$, and the close to unity value of the latter in the water proximity, all demonstrate the influence of the w.c. velocity perturbations and their mutual interaction with turbulence, through alterations in the Stokes- and critical-layer behaviour, on the bursting cycle. Notable changes in the distributions of the fractional contributions to the mean Reynolds stress and of the ratio $\overline{uv}_2/\overline{uv}_4$ occur when $c/U_{\delta_0} < 0.68$. There, the ratio $\overline{uv}_2/\overline{uv}_4$ decreases slightly with decreasing dimensionless wave speed making sweep contributions even greater. These increased sweep contributions persist irrespective of hole size (figure 8), as has also been observed in open-channel flows over rough beds.

As described earlier, the mean ejection periods (in seconds) are closely related to the time interval between the two largest consecutive peaks found in the phase-averaged distributions of the total Reynolds stress. The position of these peaks is also determined by the dynamic behaviour of critical and Stokes layer, as the dimensionless wave speed changes.

When $c/U_{\delta_0} > 1.0$, $\theta_{\tilde{u}} = 132°$ and $\theta_{\tilde{v}} = 277°$. Therefore, the two largest consecutive peaks in the $\langle uv \rangle$ stress distributions, which correspond to the ejection stage, are located on the leeward side of the mechanically generated wave crest. The subsequent two largest peaks correspond to the sweeping stage of the cycle, since for both of them $\langle u \rangle > 0$ and $\langle v \rangle < 0$, and are located on the windward side of the (long) wave crest. When $0.39 \leqslant c/U_{\delta_0} < 1.0$, $\theta_{\tilde{u}}$ and $\theta_{\tilde{v}}$ are such that the two largest consecutive peaks, which correspond to the ejection stage, shift downwind on the leeward side of the crest, whereas the other two shift upwind (and remain) on the windward side of the crest, as the dimensionless wave speed decreases. There is evidence (see, for example, Wu, Hsu & Street 1977) that for laboratory flows over purely wind-generated waves (for which $c/u_* \approx O(1)$) $\theta_{\tilde{u}} = 320$–$350°$ and $\theta_{\tilde{v}} = 285$–$295°$. Then, it is expected that the two largest consecutive peaks of the $\langle uv \rangle$ distributions, associated with ejections, will be located on the windward side of the dominant wave crest, with the other two largest peaks (associated with sweeps) being located on the leeward side of the crest. The measurements of Kawamura & Toba (1985), which show the occurrence of large negative spikes in the instantaneous $u(t)\,v(t)$ signal and large positive spikes in the instantaneous spanwise vorticity signal at fixed positions relative to the dominant wave crest, do confirm the above observation. Further evidence for the shifting behaviour of the four largest peaks of the phase-averaged $\langle uv \rangle$ stress distributions can be found in the measurements of McIntosh *et al.* (1975) over mechanically generated waves (though under slightly unstable conditions) for which $c/u_* \approx 4.0$. As with the case of purely wind-generated waves, these measurements show that the two largest consecutive peaks, associated with ejections, are also located on the windward side of the mechanically generated wave crest. It would be interesting to determine the value of c/u_* and/or any other critical parameter that influences such shifting around the dominant wave crest, and future studies should address this issue.

It is possible that in a burst of generation of turbulence, the different scales of local instability may interact so as to mutually enhance each others growth rate, smaller scales occurring preferentially at certain phases of the larger scales on which they ride to allow their Reynold stress to do work on the larger scales, while the larger scales through their growth make the smaller-scale instability persist. The processes whereby the smaller-scale disturbances focus at certain phases of the larger scales may be as described by Landahl (1972). The experiments of Kendall (1970) and of Hussain & Reynolds (1970) do show that a rigid wavy boundary affects the generation of turbulence and the structure of a turbulent field, and that the phase velocity of the waves affects the generation and response of the turbulent field. The experiments on the structure of air flow above water waves described in Hsu & Hsu (1983), I and elsewhere all show that the air–water interface, in response to the external (wind) forcing, definitely affects the dynamics of the small-scale turbulence and produces coupling between scales.

5. Summary and conclusions

A set of experiments was conducted to study the influence of mechanically generated water waves on the bursting cycle. Based on the results and discussion presented, the following conclusions can be drawn.

The presence of mechanically generated water waves affects the mechanism of Reynolds stress production through variations in the dynamic behaviour of the critical and Stokes layers in the air, and their mutual interaction. At high

dimensionless wave speeds (i.e. $c/U_{\delta_0} \geqslant 0.68$ or $c/u_* > 20$), most of the flow in the turbulent boundary layer is below the critical height, the nonlinear critical-layer thickness is large compared with the wave amplitude, and such alterations result from the thickening of the Stokes layer by turbulence diffusion and mixing; this process stimulates the production of the w.a. stresses by the Stokes layer. At low dimensionless wave speeds (i.e. $c/U_{\delta_0} < 0.68$ or $c/u_* < 20$), most of the flow in the boundary layer is above the critical height, the nonlinear critical-layer thickness is small compared with the wave amplitude, and the compression of the Stokes layer by the vortex force, acting on the vortical layer associated with the cat's eye pattern, results in a weak production of the w.a. stresses by the Stokes layer; however, the compression of the flow field below the critical height may enhance the production of the w.a. stress in the critical layer. Owing to the modifications of the w.c. flow by the critical and Stokes layers, the bursting events are also enhanced in the presence of mechanically generated waves. Throughout the boundary layer, ejections are the largest contributor to the mean Reynolds stress, with sweeps being the second largest. In the water proximity, when $c/U_{\delta_0} \geqslant 0.68$, ejections and sweeps contribute about 90% and 77% to $\overline{uv}$, whereas the outward and inward interactions contribute -34% and -33%, respectively. When $c/U_{\delta_0} < 0.68$, a pronounced rise in the fractional contributions of the bursting events to $\overline{uv}$ is observed. The w.a. stress counterbalances this rise and results in constant fractional contributions $\overline{u'v'_j}/\overline{u'v'}$ ($j = 1, 2$), independent of dimensionless wave speed. The value of $\mu_c = c/U_{\delta_0}$ (≈ 0.68 in this study) which appears to distinguish the flow regimes of high and low critical layer, and is associated with significant and weak production of the w.a. stress, is not a universal constant but may depend on: (i) the wave age (c/u_*); (ii) the wave slope, or significant slope as defined by Huang *et al.* (1981), (ka); and (iii) the non-dimensional fetch (xg/u_*^2), parameters that express the wind and wave field conditions and their mutual coupling. Future attempts should address this aspect, by conducting experiments under a variety of wind and wave conditions.

Close to the water surface, sweeps and ejections contribute about equally to the mean Reynolds stress $\overline{uv}$ (i.e. $\overline{uv}_2 \approx \overline{uv}_4$), at all dimensionless wave speeds, while the height distribution of their relative contributions, $\overline{uv}_i/\overline{uv}$, does vary with c/U_{δ_0}. The width of the zone of influence of the surface waves on these distributions is basically determined by the ratio c/u_*, the wave Reynolds number R_w, and the dimensionless nonlinear critical-layer thickness $k\delta_m$. In the outer part of the equilibrium region and close to the free stream, the bursting process consists of smoother and more isotropic events with a universal character independent of flow type and surface roughness condition.

The mean time interval between ejections or sweeps does not scale with either the inner or outer flow variables. However, the mean ejection period can be determined from the time between the two largest consecutive peaks of the phase-averaged Reynolds stress distribution.

For $0.39 \leqslant c/U_{\delta_0} \leqslant 1.0$, ejections and sweeps occur on the leeward and windward side of the mechanically generated wave crest, respectively. Such a behaviour, however, cannot be regarded as universal, because for air flows above purely wind-generated waves (where $c/U_{\delta_0} \ll 1.0$ and $c/u_* = O(1)$) ejections and sweeps usually occur on the windward and leeward side of the dominant wave crest.

When normalized with $\kappa y^*/u_*^3$, the total energy production, owing to w.c. contributions, shows a peak near the water surface with a maximum value of ≈ 3.8, at the highest dimensionless wave speed (where $c/U_{\delta_0} > 1.0$). The normalized turbulence energy production, however, is smallest at this dimensionless wave speed.

This peak decreases in magnitude with decreasing c/U_{δ_0}, and disappears as c/U_{δ_0} becomes smaller than 0.68.

This work was supported by the National Science Foundation through Grant NSF-CEE-7817618. The authors are also indebted to the referees, and particularly to Dr F. Dobson, for their valuable comments and suggestions. R.L.S. has also received support from the Office of Naval Research under contract N00014-84-K-0242.

REFERENCES

ALFREDSSON, P. H. & JOHANSSON, A. V. 1982 Time scales for turbulent channel flow. *Royal Inst. Tech., Stockholm, Rep.* TRITA-MCK-82-11.

ALFREDSSON, P. E. & JOHANSSON, A. V. 1983 Effects of imperfect spatial resolution on measurements of wall-bounded turbulent shear flows. *J. Fluid Mech.* **137**, 409.

ANTONIA, R. A. B. & CHAMBERS, A. J. 1980 Wind-wave-induced disturbances in the marine surface layer. *J. Phys. Oceanogr.* **10**, 611.

BENJAMIN, T. B. 1959 Shearing flow over a wavy boundary. *J. Fluid Mech.* **6**, 161.

BENNEY, D. J. & BERGERON, R. R. J. 1969 A new class of nonlinear waves in parallel flows. *Stud. Appl. Maths.* **48**, 181.

BLACKWELDER, R. F. & HARITONIDIS, J. H. 1983 Scaling of the bursting frequency in turbulent boundary layers. *J. Fluid Mech.* **132**, 87.

BLACKWELDER, R. F. & KAPLAN, R. E. 1972 Intermittent structures in turbulent boundary layers. *NATO-AGARD* CP93. London Technical Editing and Reproduction.

BOGARD, D. G. & TIEDERMAN, W. G. 1983 Investigation of flow visualization techniques for detecting turbulent bursts. *Symposium on Turbulence*, 1981, p. 289. University of Missouri-Rolla.

BOGARD, D. G. & TIEDERMAN, W. G. 1986 Burst detection with single-point velocity measurements. *J. Fluid Mech.* **162**, 389.

BRADSHAW, P. 1978 *Topics in Applied Physics–Turbulence.* Springer.

BRODKEY, R. S., WALLACE, J. M. & ECKELMANN, H. 1974 Some properties of truncated turbulence signals in bounded shear flows. *J. Fluid Mech.* **63**, 209.

BUCKLES, J., HANRATTY, T. S. & ADRIAN, R. J. 1984 Turbulent flow over large-amplitude wavy surfaces. *J. Fluid Mech.* **140**, 27.

BUSCH, N. E. 1973 On the mechanics of atmospheric turbulence. In *Workshop on Micrometeorology* (ed. D. A. Haugen), p. 1. AMS Science Press.

CEBECI, T. & BRADSHAW, P. 1977 *Momentum Transfer in Boundary Layers.* McGraw-Hill.

CHALIKOV, D. V. 1986 Numerical simulation of the boundary layer above waves. *Boundary-Layer Met.* **34**, 63.

CHAMBERS, A. J. & ANTONIA, R. A. 1981 Wave-induced effect on the Reynolds shear stress and heat flux in the marine surface layer. *J. Phys. Oceanogr.* **11**, 116.

CHEN, C. H. P. & BLACKWELDER, R. F. 1978 Large-scale motion in a turbulent boundary layer: a study using temperature contamination. *J. Fluid Mech.* **89**, 1.

CHEUNG, T. K. 1985 A study of the turbulent boundary layer in the water at an air–water interface. *Dept. Civil Engng., Stanford Univ., Tech. Rep.* 287.

CORINO, E. R. & BRODKEY, R. S. 1969 A visual investigation of the wall region in turbulent flow. *J. Fluid Mech.* **37**, 1.

CSANADY, G. T. 1985 Air–sea momentum transfer by means of short-crested wavelets. *J. Phys. Oceanogr.* **15**, 1488.

DAVIS, R. E. 1969 On the high Reynolds number flow over a wavy boundary. *J. Fluid Mech.* **36**, 337.

DORMAN, C. E. & MOLLO-CHRISTENSEN, E. 1973 Observations on the structure of moving gust patterns over a water surface (cats paws). *J. Phys. Oceanogr.* **3**, 120.

ELLIOTT, J. A. 1972 Microscale pressure fluctuations near waves being generated by the wind. *J. Fluid Mech.* **54**, 427.

GRASS, A. J. 1971 Structural features of turbulent flow over smooth and rough boundaries. *J. Fluid Mech.* **50**, 233.

HINZE, J. O. 1975 *Turbulence* (2nd edn), p. 586. McGraw-Hill.

HSU, C. T. & HSU, E. Y. 1983 On the structure of turbulent flow over a progressive water wave: theory and experiment in a transformed wave-following coordinate system. Part 2. *J. Fluid Mech.* **131**, 123.

HSU, C. T., HSU, E. Y. & STREET, R. L. 1981 On the structure of turbulent flow over a progressive water wave: theory and experiments in a transformed wave-following coordinate system. Part 1. *J. Fluid Mech.* **105**, 87.

HSU, C. T., WU, H.-Y., HSU, E. Y. & STREET, R. L. 1982 Momentum and energy transfer in wind generation of waves. *J. Phys. Oceanogr.* **12**, 929.

HUANG, N. E., LONG, S. R. & BLIVEN, L. F. 1981 On the importance of significant slope in empirical wind-wave studies. *J. Phys. Oceanogr.* **11**, 569.

HUSSAIN, A. K. M. F. & REYNOLDS, W. C. 1970 The mechanics of an organized wave in turbulent shear flow. *J. Fluid Mech.* **41**, 241.

JACKSON, R. G. 1976 Sedimentological and fluid-dynamic implications of the turbulent bursting phenomenon in geophysical flows. *J. Fluid Mech.* **77**, 531.

KAWAI, S. 1981 Visualization of air flow separation over wind wave crests under moderate wind. *Boundary-Layer Met.* **21**, 93.

KAWAI, S. 1982 Structure of air flow separation over wind wave crests. *Boundary-Layer Met.* **23**, 503.

KAWAMURA, H., OKUDA, K., KAWAI, S. & TOBA, Y. 1981 Structure of turbulent boundary layer over wind waves in a wind tunnel. *Tohoku Geophys. J. (Sci. Rep. Tohoku Univ., Ser* 5) **28**, 69.

KAWAMURA, H. & TOBA, Y. 1985 New aspects of the turbulent boundary layer over wind waves. In *The Ocean Surface. Wave Breaking, Turbulent Mixing and Radio Probing* (ed. Y. Toba & H. Mitsuyasu), p. 105. Reidel.

KENDALL, J. M. 1970 The turbulent boundary layer over a wall with progressive surface waves. *J. Fluid Mech.* **41**, 259.

KIM, H. T., KLINE, S. J. & REYNOLDS, W. C. 1971 The production of turbulence near a smooth wall in a turbulent boundary layer. *J. Fluid Mech.* **50**, 133.

KINSMAN, B. 1965 *Wind Waves: Their Generation and Propagation on The Ocean Surface.* Prentice Hall.

KLINE, S. J., REYNOLDS, W. C., SHRAUB, F. A. & RUNSTANDLER, P. W. 1967 The structure of turbulent boundary layers. *J. Fluid Mech.* **30**, 741.

KITAIGORODSKII, S. A. & DONELAN, M. A. 1984 Wind wave effects on gas transfer. In *Gas Transfer at Water Surfaces* (ed. W. Brutsaert & G. H. Jirka), p. 147. Reidel.

LANDAHL, M. T. 1972 Wave mechanics of breakdown. *J. Fluid Mech.* **56**, 775.

LAUFER, J. 1975 New trends in experimental turbulence research. *Ann. Rev. Fluid Mech.* **7**, 307.

LIGHTHILL, M. J. 1962 Physical interpretation of the mathematical theory of wave generation by wind. *J. Fluid Mech.* **14**, 385.

LIGRANI, P. M. & MOFFAT, R. J. 1986 Structure of transitionally rough and fully rough turbulent boundary layers. *J. Fluid Mech.* **162**, 69.

LIN, C. C. 1955 *The Theory of Hydrodynamic Stability.* Cambridge University Press.

LONGUET-HIGGINS, M. S. 1969 Action of a variable stress at the surface of water waves. *Phys. Fluids* **12**, 737.

LU, S. S. & WILLMARTH, W. W. 1972 The structure of the Reynolds stress in a turbulent boundary layer. *Dept. Aerospace Engng., University of Michigan, ORA Rep.* 021490-2-T.

LU, S. S. & WILLMARTH, W. W. 1973 Measurements of the structure of the Reynolds stress in a turbulent boundary layer. *J. Fluid Mech.* **60**, 481.

MCINTOSH, D. A., STREET, R. L. & HSU, E. Y. 1975 Turbulent heat and momentum transfer at an

air–water interface: the influence of surface conditions. *Dept. Civil Engng., Stanford Univ., Tech. Rep.* 197.

MILES, J. W. 1957 On the generation of surface waves by shear flows. *J. Fluid Mech.* **3**, 185.

MILES, J. W. 1959 On the generation of surface waves by shear flows. Part 2. *J. Fluid Mech.* **6**, 568.

MOLLO-CHRISTENSEN, E. 1973 Intermittency in large scale turbulent flows. *Ann. Rev. Fluid Mech.* **5**, 101.

MORDUCKHOVICH, M. I. & TSVANG, L. R. 1966 Direct measurements of turbulent flows in two heights in the atmospheric layer. *Izv. Atmos. Ocean. Phys.* **2**, 477.

NAKAGAWA, H. & NESU, I. 1977 Prediction of the contributions to the Reynolds stress from bursting events in open channel flows. *J. Fluid Mech.* **80**, 99.

NAKAGAWA, H. & NESU, I. 1981 Structure of space–time correlations of bursting phenomena in an open-channel flow. *J. Fluid Mech.* **104**, 1.

OFFEN, G. R. & KLINE, S. J. 1975 A comparison and analysis of detection methods for the measurements of production in a boundary layer. *Proc. 3rd Biennial Sympos. on Turbulence in Liquids, University of Missouri-Rolla*, p. 289.

OKUDA, K. 1983 Internal flow structure of short wind waves. Part III. Pressure distributions. *J. Ocean Soc. Japan* **38**, 331.

PAPADIMITRAKIS, Y. A. 1982 Velocity and pressure measurements in the turbulent boundary layer above mechanically-generated water waves. Ph.D. dissertation, Dept. Civil Engng., Stanford University.

PAPADIMITRAKIS, Y. A., HSU, E. Y. & STREET, R. L. 1984 On the structure of the velocity field over progressive, mechanically-generated water waves. *J. Phys. Oceanogr.* **14**, 1937.

PAPADIMITRAKIS, Y. A., HSU, E. Y. & STREET, R. L. 1985 On the resolution of organized spurious pressure fluctuations in wind-wave facilities. *J. Acoust. Soc. Am.* **77**, 986.

PAPADIMITRAKIS, Y. A., HSU, E. Y. & STREET, R. L. 1986 The role of wave-induced pressure fluctuations in the transfer processes across an air–water interface. *J. Fluid Mech.* **170**, 113.

PAPADIMITRAKIS, Y. A., HSU, Y.-H. L. & WU, J. 1986 Turbulent heat and mass transfers across a thermally stratified air–water interface. *J. Geophys. Res.* **91**, 10607.

PAPADIMITRAKIS, Y. A., HSU, Y.-H. L. & WU, J. 1987 Thermal stability effects on the structure of the velocity field above an air–water interface. *J. Geophys. Res.* **92**, C8, 8277.

PHILLIPS, O. M. 1977 *The Dynamics of the Upper Ocean.* Cambridge University Press.

RAO, K. N., NARASIMHA, R. & BADRI NARAYANAN, M. A. 1971 The bursting phenomenon in a turbulent boundary layer. *J. Fluid Mech.* **48**, 339.

ROBINSON, J. L. 1974 The inviscid nonlinear instability of parallel/shear flows. *J. Fluid Mech.* **63**, 723.

SCHRAUB, F. A., KLINE, S. J., HENRY, J., RUNSTADLER, P. W. J. & LITTEL, A. 1965 Use of hydrogen bubbles for quantitative determination of time-dependent velocity fields in low-speed water flows. *Trans. ASME* D: *J. Basic Engng* **87**, 429.

SHEMDIN, O. H. & LAI, R. J. 1973 Investigation of the velocity field over waves using a wave follower. *Tech. Rep.* 18. Coastal and Ocean Engng Lab, University of Florida.

SNYDER, R. L., DOBSON, F. W., ELLIOTT, J. A. & LONG, R. B. 1981 Array measurements of atmospheric pressure fluctuation above surface gravity waves. *J. Fluid Mech.* **102**, 1.

STREET, R. L. 1979 Turbulent heat and mass transfer across a rough air–water interface: a simple theory. *Intl J. Heat Mass Transfer* **22**, 885.

TAKEUCHI, K., LEAVITT, E. & CHAO, S. P. 1977 Effects of water waves on the structure of turbulent shear flow. *J. Fluid Mech.* **80**, 535.

TIEDERMAN, W. G., SMITH, A. J. & OLDAKER, D. K. 1977 Structure of the viscous sublayer in drug-reducing channel flows. In *Proc. 4th Biennial Sympos. On Turbulence in Liquids, University of Missouri-Rolla*, p. 312.

TOBA, Y., KAWAMURA, H. & OKUDA, K. 1984 Ordered motions in turbulent boundary layers above and below wind waves. In *Turbulence and Chaotic Phenomena in Fluids* (ed. T. Tatsumi), p. 513. Elsevier, IUTAM.

WALLACE, J. M., ECKELMANN, H. & BRODKEY, R. S. 1972 The wall region in turbulent shear flow. *J. Fluid Mech.* **54**, 39.

WARHAFT, Z. & BOLGIANO, R. J. 1984 Moisture and heat transport in a stably stratified boundary layer over a water surface. In *Gas Transfer at Water Surfaces* (ed. W. Brutsaert & G. H. Jirka), p. 133. Reidel.

WILLMARTH, W. W. 1975 Structure of turbulence in a boundary layer. *Adv. Appl. Mech.* **15**, 159.

WU, H.-Y., HSU, E. Y. & STREET, R. L. 1977 The energy transfer due to air input, non linear wave–wave interaction and white-cap dissipation associated with wind-generated waves. *Dept. Civil Engng, Stanford Univ. Tech. Rep.* 207.

VOLKOV, Y. A. 1970 Turbulent flux of momentum and heat in the atmospheric surface layer over a disturbed sea-surface. *Izv. Atmos. Ocean. Phys.* **6**, 1295.